

Inhibition Mechanism of Some Vinylalkylimidazolium-Based Polymeric Ionic Liquids against Acid Corrosion of API 5L X60 Steel: Electrochemical and Surface Studies

Giselle Gómez-Sánchez, Octavio Olivares-Xometl,* Natalya V. Likhanova, Paulina Arellanes-Lozada,* Irina V. Lijanova, Víctor Díaz-Jiménez, Diego Guzmán-Lucero, and Janette Arriola-Morales



Cite This: *ACS Omega* 2022, 7, 37807–37824



Read Online

ACCESS |



Metrics & More

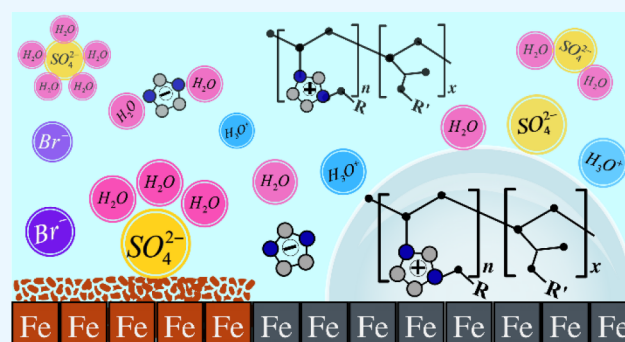


Article Recommendations



Supporting Information

ABSTRACT: A corrosion inhibition mechanism of API 5L X60 steel exposed to 1.0 M H_2SO_4 was proposed from the evaluation of three vinylalkylimidazolium poly(ionic liquids) (PILs), employing electrochemical and surface analysis techniques. The synthesized PILs were classified as mixed-type inhibitors whose surface adsorption was promoted mainly by bromide and imidazolate ions, which along with vinylimidazolium cations exerted a resistive effect driven by a charge transfer process by means of a protective PIL film with maximal efficiency of 85% at 175 ppm; the steel surface displayed less surface damage due to the formation of metal–PIL complex compounds.



1. INTRODUCTION

Corrosion is a process that implies not just economic losses but also potential risks that expose the safety of chemical processes and, as a consequence, the integrity and equilibrium of human and natural and environmental resources; for these reasons, its in-advance control is of the utmost importance.^{1,2} Particularly, carbon steel is a material that is widely employed in industrial complexes due to its many advantageous features, but unfortunately, it is easily damaged by the corrosion phenomenon. Its decay is promoted by its being in contact with corrosive solutions through acid cleaning, pickling of metallic samples, or acidification processes for enhancing oil production.³ In this context, effective strategies for controlling and mitigating the corrosion of carbon-steel-based systems are required; to this end, the application of corrosion inhibitors (CIs) has stood out as one of the most economic and efficient methods aimed at fighting this problematic situation.⁴ CIs work by diminishing the corrosion process suffered by a metallic substrate in a given medium.⁵

As for film-forming CIs, they work through physisorption, chemisorption, or physisorption–chemisorption processes on a metallic surface, thus decreasing its interaction with the aggressive medium.⁶ Different research works have reported that organic CIs have proven to be effective for this purpose due to the presence of heteroatoms with high electron density (N, S, O, P) with unpaired and π electrons that interact, mainly, with the vacant Fe d orbital.^{7–11} Likewise, it has been found that CIs with heterocyclic aromatic groups such as imidazole, pyridine, pyrrolidone, and thiazole, among others, have turned out to be

efficient against corrosion because of their polar functional groups like primary amines (NH_2), secondary amines (NH), and carbonyl groups ($\text{C}=\text{O}$) whose double bonds improve the interaction with the metallic surface.¹²

Recently, poly(ionic liquids) (PILs) have become especially interesting due to their functionality as ion-conducting electrolytes,¹³ being useful in different fields such as analytic chemistry, biotechnology, and energy and environmental applications. The outstanding potential of PILs has allowed the development of new ion types stemming from ionic liquids (ILs) because of the possibility of selecting polymeric segments that enrich their properties.^{14,15} According to reported results, PILs can be employed as CIs in acidic media.^{4,16} As for the ionic feature of PILs, it depends on the chemical nature of both the polymeric structure and counterion. It is worth emphasizing that imidazolium cations possess the highest ionic conductivities in comparison with those of pyrrolinium, pyrrolidonium, tetraalkylammonium, and piperidinium.¹⁷ Regarding halide anions, tetrafluoroborate, sulfonates, or hexafluorophosphate, they also present high ionic activities.¹⁸ It has been found that CIs with halide ions (Cl^- , Br^- , I^-) are capable of inhibiting the steel acid corrosion because they trigger a synergistic effect between the

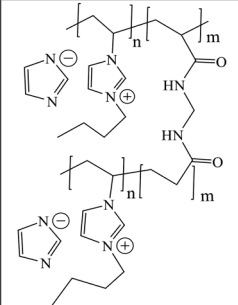
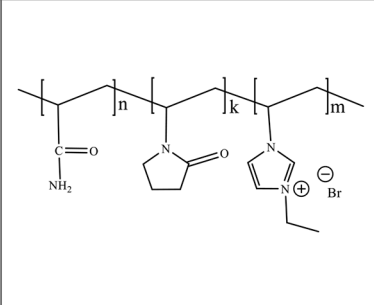
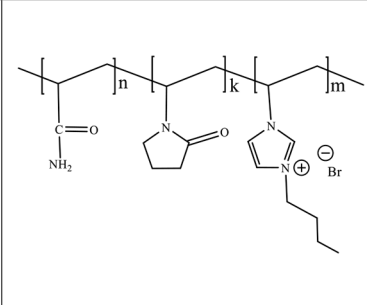
Received: July 28, 2022

Accepted: October 4, 2022

Published: October 14, 2022



Table 1. Chemical Structures of PILs Evaluated as CIs

		
Poly (1-butyl-3-vinylimidazolium) imidazolate, Poly [VIMC4][Im]	Poly (acrylamide-N-vinylpyrrolidone-1-ethyl-3-vinylimidazolium bromide), Poly [VIMC2][Br]	Poly (acrylamide-N-vinylpyrrolidone-1-butyl-3-vinylimidazolium bromide), Poly [VIMC4][Br]

halide ions and inhibiting molecules by forming bridges between the positively charged metal surface and the cation of the inhibiting molecule, thus improving the covering of the steel surface by means of the cation–anion pair interaction.¹⁹ One of the disadvantages of employing ILs as CIs is that they display unfavorable transport properties due to their miscibility with the medium; for this reason, PILs are considered as more suitable than their monomers alone because their polymeric nature provides high performance in saline media, high thermal and shear stress stability, and high resistance to strong acids.^{20,21} In addition, they present self-assembly properties and mechanical stability in aqueous media; likewise, they possess multiple adsorption centers that ease their adhesion on the metallic surface by occupying a higher surface area due to their high molecular weight, which contributes to the protection of the material before aggressive agents.²² The most commonly employed polymeric CIs are derived from polyamines and polyvinylamides, polyaspartates, polyamino acids, polycarboxylates, and polysulfides, among others.²³ Umoren et al. evaluated polymers with polyvinylpyrrolidone and polyacrylamide in sulfuric acid at temperatures ranging from 30 to 60 °C and reported that these compounds were more efficient at low temperatures through physical adsorption from their O and N heteroatoms as the main adsorption centers. In acidic medium, they can be protonated through the carbonyl group to form a polycation in the PIL.²⁴ Likewise, Khairou et al. found that the hydroxy and carboxyl groups present in sodium polyacrylate and polyacrylamide contributed positively to their efficiency as CIs, concluding that these compounds possess hydrophilic properties and participate in slowing the anodic dissolution process.²⁵ In contrast, Kamali et al. performed the study of poly(3-butyl-1-vinylimidazolium bromide), suggesting that the adsorption of the PIL molecules modified the electric double layer on the steel surface in HCl by blocking anodic sites in the metal–solution interface; thus, a spontaneous adsorption process took place by electrostatic forces between the PIL and metal surface, modifying the hydrogen evolution mechanism.²⁶ It is worth mentioning that some PILs have also been evaluated in other corrosive media as reported by Likhanova et al. in their study of PILs derived from alkylimidazolium and imidazolate in production water. The authors suggest that the compounds were adsorbed on the metal surface due to their high molecular weight and orientation of the lateral alkyl groups in the PIL cations, creating hydrophobic interactions that diminished the diffusion process of water molecules and/or corrosive ions toward the metal surface.²⁷

In the present work, three PILs with different IL species (Table 1) were evaluated in the corrosion inhibition of API 5L X60 steel in 1 M H₂SO₄: poly(1-butyl-3-vinylimidazolium) imidazolate (poly[VIMC4][Im]), poly(acrylamide-N-vinylpyrrolidone-1-ethyl-3-vinylimidazolium bromide) (poly[VIMC2][Br]), and poly(acrylamide-N-vinylpyrrolidone-1-butyl-3-vinylimidazolium bromide) (poly[VIMC4][Br]). The inhibition efficiency was studied from electrochemical techniques like linear polarization resistance (LPR), potentiodynamic polarization (PDP), and electrochemical impedance spectroscopy (EIS); surface analyses such as scanning electron microscopy (SEM) and X-ray photoelectron spectroscopy (XPS) were also carried out to elicit a mechanism describing the corrosion inhibition mechanism of steel exposed to an acid medium in the presence of PILs.

2. RESULTS AND DISCUSSION

2.1. Electrochemical Behavior. Figure 1 shows the open-circuit potential values (E_{OCP}) of API 5L X60 steel in 1 M H₂SO₄ in the absence and presence of different PIL concentrations. It can be observed that as the CI concentration increases the E_{OCP} values are slightly displaced toward more positive values, in contrast with the blank value, which is associated with the formation of an inhibitor film on the metal surface. The PILs showed E_{OCP} in different intervals from 445 to 462 mV for poly[VIMC4][Im], from 450 to 455 mV for poly[VIMC2][Br], and from 451 to 458 mV for poly[VIMC4][Br]. The E_{OCP} stability of API 5L X60 steel in 1 M H₂SO₄ in the absence and presence of PILs was observed after 600 s.

The Rp behavior pattern in the presence of PILs obtained by LPR is shown in Figure 2. It was found that as the inhibitor concentration (C_{INH}) was increased the current density (i) vs overpotential (η) slopes diminished, which implies higher Rp and suggests that the inhibition process on the steel surface occurred through the adsorption of PIL molecules.^{28,29} This effect is also shown in Figure 3 from the PDP behavior with respect to $\log i$ and C_{INH} . The decrease of $\log i$ with C_{INH} indicates that the PILs worked as CIs, yielding values below 175 ppm of poly[VIMC4][Im], poly[VIMC2][Br], and poly[VIMC4][Br]. Notwithstanding, these changes were minimal at $C_{\text{INH}} \geq 100$ ppm. These results confirm that the addition of PILs to 1 M H₂SO₄ at 25 °C exerts a protection effect on the metal surface by diminishing the corrosion rate (v_{corr}) of API 5L X60 steel; in other words, the use of PILs retarded the hydrogen evolution reactions and iron dissolution.³⁰

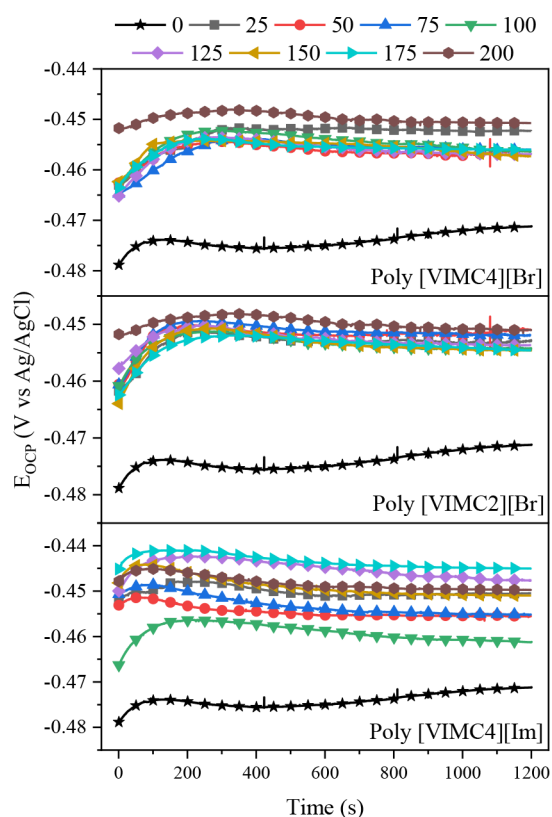


Figure 1. E_{OCP} plots as functions of time of API 5L X60 steel in 1 M H_2SO_4 in the absence and presence of PILs.

The plots also show the displacement of the corrosion potential (ΔE_{corr}) in the presence of PILs in an acid medium with respect to the blank; it is observed that at higher C_{INH} there is an effect on the E_{corr} of the steel surface whose computation is defined by eq 1,³¹ where the potentials are considered in the presence ($E_{\text{corr}}^{\text{inh}}$) and absence (E_{corr}^0) of CIs:

$$\Delta E_{\text{corr}} = E_{\text{corr}}^{\text{inh}} - E_{\text{corr}}^0 \quad (1)$$

The ΔE_{corr} results obtained for the evaluated systems were the following: poly[VIMC4][Im] from 8 to 25 mV, poly[VIMC2]-[Br] from 15 to 20 mV, and poly[VIMC4][Br] from 11 to 18 mV. According to the literature, the ΔE_{corr} values correspond to the behavior of mixed-type CIs; this statement was supported by the presence of displacements below ± 85 mV with respect to the blank³² and anodic preference for ΔE_{corr} positive values, which is associated with a higher contribution of bromide $[\text{Br}^-]$ or imidazolate $[\text{Im}^-]$ anions to the adsorption process. The CI mixed-type behavior indicates that the PILs can retard both cathodic and anodic reactions by blocking the active sites on the metal surface.³³

As for the anodic branches of the PDP plots (Figure 3), it can be observed that they do not feature the required linearity for calculating the anodic slope (β_a), which is related to the reorientation of the cation heteroatoms from the IL species present in the polymeric structure and/or to the formation of corrosion products on the steel surface such as iron sulfates and/or iron oxyhydroxides.^{34,35} In contrast, the cathodic branches display the typical linear Tafel pattern, which indicates that the hydrogen evolution was controlled by activation through cationic species (vinyl alkylimidazolium) or by amide functional groups (pyrrolidone and/or acrylamide) that were adsorbed on the steel cathodic sites, thus inhibiting the corrosion reaction.

The adsorption on anodic sites occurred from the $[\text{Im}^-]$ or $[\text{Br}^-]$ anionic species and/or from carbonyl functional groups ($\text{C}=\text{O}$) present in the evaluated PILs that retarded the steel dissolution.³⁶

Table 2 shows the LPR and PDP electrochemical parameters for API 5L X60 steel exposed to 1 M H_2SO_4 and PILs. The Rp values were obtained with the reciprocal value of the i vs η slopes; regarding the PDP parameters, the intersection of the E_{OCP} values with the linear extrapolation of the cathodic branches was used.³⁷ The Rp increase and i_{corr} decrease in the presence of CIs are associated with the formation of a film of adsorbed PIL molecules that limited the interaction between the metal surface and medium corrosive ions such as hydronium (H_3O^+), sulfate (SO_4^{2-}), and the water molecule, thus favoring the diminution of v_{corr} of API 5L X60 steel.³⁸ It can also be observed that the cathodic slopes (β_c) do not show a defined behavior pattern with respect to C_{INH} . As discussed previously, this parameter is associated with the delay of the hydrogen generation in the cathodic zone.³⁹

The obtained IE values for LPR and PDP were directly proportional to C_{INH} and fell within the interval ranging from 41 to 85%. The PILs poly[VIMC4][Im], poly[VIMC2][Br], and poly[VIMC4][Br] reached IE_{max} values of 77, 84, and 85% at 175 ppm, respectively. Poly[VIMC4][Im] did not present a significant variation of IE ($<10\%$) as a function of C_{INH} from 100 ppm, which was attributed to the surface saturation with PIL molecules, thus limiting the adsorption process.

The Nyquist and Bode diagrams of API 5L X60 steel in 1 M H_2SO_4 in the presence and absence of PILs at 25 °C are shown in Figure 4. The Nyquist spectra (Figure 4a–c) display the impedance results ($Z = Z' + jZ''$) formed by the real (Z') and imaginary ($-Z''$) parts, where depreciated semicircles with center below the real axis and consisting of a capacitive loop that becomes outstanding at high frequencies can be distinguished; these facts indicate that the steel corrosion was controlled by a charge transfer process. In the presence of CI, it is observed that the diameter in Z' was increased with respect to the blank. Additionally, a small inductive loop is present at low frequencies,⁴⁰ which can be attributed to the surface heterogeneous nature promoted by the acid corrosion and impurities present in the metal sample. This characteristic is also associated with adsorption or desorption processes of species coming from the $\text{H}_2\text{SO}_{4(\text{aq})}$ –PIL system.⁴¹

The addition of CIs to the acid medium modified the steel impedance through the increase of Z' at low frequencies, which is represented by the diameter growth of the semicircles with the increase in C_{INH} . This fact suggests that the amount of PIL molecules present in the corrosive solution is directly proportional to the impedance of the steel sample. Such an effect is also related to a higher resistance of charge transfer in the metal–solution interphase due to the adsorption of CI molecules that limited the migration of H_3O^+ and SO_4^{2-} ions toward the metallic interphase.⁴²

In contrast, the Bode diagrams (Figures 4d–f) present a double axis consisting of the impedance module $|Z|$ and the phase angle ϕ , both variables as functions of the frequency f . The plots show a displacement toward higher $|Z|$ values in the presence of PILs with respect to the blank, which suggests that the evaluated CIs retarded the redox reactions of the corrosion process of API 5L X60 steel in an acid medium.⁴³

The behavior of f in the absence and presence of the PILs was as follows: at low f values (from 10^{-1} to 10^1 Hz), it is observed that $|Z|$ presented an approximate increase from 20 to 200 $\Omega \text{ cm}^2$

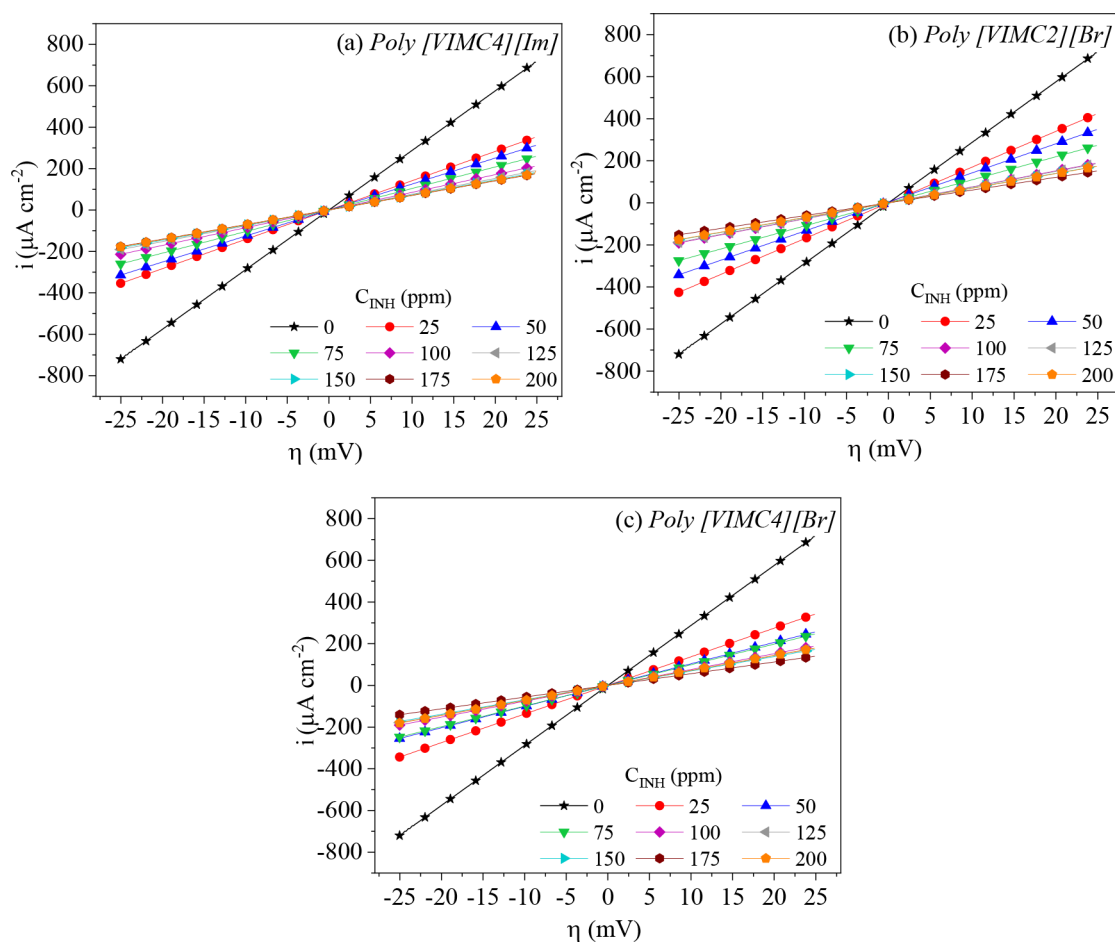


Figure 2. LPR behavior of API 5L X60 steel in 1 M H₂SO₄ in the presence of (a) poly[VIMC4][Im], (b) poly[VIMC2][Br], and (c) poly[VIMC4][Br] at 25 °C.

with respect to the blank; this fact suggests the occurrence of charge transfer, mass transfer, or surface relaxation processes associated with the adsorption of the CIs.⁴⁴ In the region of intermediate f (from 10^1 to 10^3 Hz), a significant $|Z|$ linear decay in the presence of PILs with respect to the blank and the formation of an ϕ_{\max} of 70° at high C_{INH} were observed, which confirmed that the film formed on the surface is related to the charge transfer resistance and capacitance of the electric double layer.^{45,46} Finally, in the high f region (from 10^3 to 10^5 Hz), constant $|Z|$ values in the presence and absence of CIs are observed, which can be related to the solution resistance. It is worth mentioning that in this region the formation of a time constant also took place.⁴⁷

The variations with respect to the blank, observed in the EIS spectra, display the charge transfer process between the metal surface and the acid–PIL system, which is associated mainly with the steel anodic dissolution process, exerting an inhibition effect through the electric double layer in the presence of PILs, thus diminishing the steel attack by H₂SO₄(aq).

The obtained EIS experimental data (Figure 4) were analyzed by employing the equivalent electrical circuit (EEC) model from Figure 5, in order to properly describe the interfacial phenomenon occurring between the steel and H₂SO₄–PIL solution.^{7,48} The proposed EEC consists of the following electrical elements: the element R_s is the solution resistance, determined by the intersection of the capacitive loop with Z' at high frequencies in the Nyquist plots; this electrical element

describes the resistance that the WE opposes to the electrolytic solution. The elements R_{ct} and CPE_{dl} represent the charge transfer process in the metal–solution interface. The first one is the charge transfer resistance, and the second one refers to the capacitive element associated with the electric double layer. R_L and L are the inductive resistance and inductance, respectively. These elements imply relaxation processes of the adsorbed species coming from the CIs and H₃O⁺ and SO₄²⁻ ions in the acid medium.⁴⁹ R_f and CPE_f represent the resistance and capacitance of the film formed on the steel surface consisting of corrosion products and/or PIL molecules.

The electrochemical parameters obtained from the EEC fitting are shown in Table 3. The R_{ct} values grew with the increasing C_{INH} , indicating that the PIL molecules are adsorbed on the steel surface, promoting a resistive effect that diminished the charge transfer. In contrast, the C_{dl} values diminished with C_{INH} , which was attributed to the decrease of the local dielectric constant of the solution and/or to the thickness increase of the electric double layer due to the displacement of water molecules and corrosive ions adsorbed on the metal surface by CI molecules.^{36,50,51}

The constant phase elements (CPEs) in an EEC are employed to represent the nonideal capacitances of the EIS spectra as observed in the depreciated circles (Figure 4). The impedance of a CPE (Z_{CPE}) can be calculated from two parameters: the proportional factor Y_0 and the exponent n . The latter is associated with the surface irregularities produced by roughness,

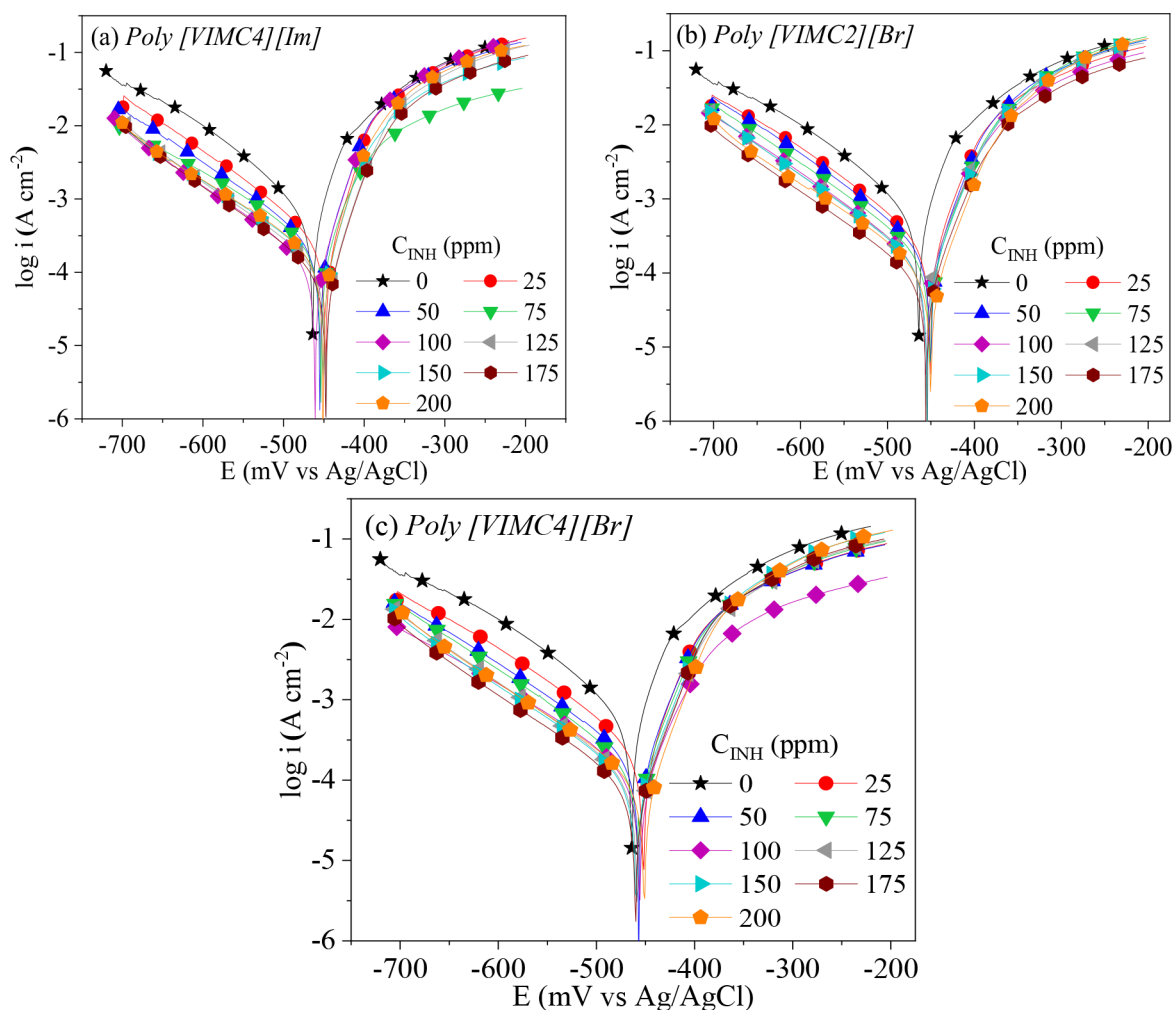


Figure 3. PDP behavior of API 5L X60 steel in 1 M H₂SO₄ in the presence of (a) poly[VIMC4][Im], (b) poly[VIMC2][Br], and (c) poly[VIMC4][Br] at 25 °C.

inhibitor adsorption, or the formation of porous layers. Z_{CPE} is defined by eq 2

$$Z_{CPE} = Y_0^{-1} \omega^{-n} \quad (2)$$

where j is an imaginary number $(-1)^{1/2}$; $\omega = 2\pi f$ is the angular frequency of the maximal value of the real impedance; and n represents the behavior deviation of an ideal capacitance within an interval of $-1 \leq n \leq 1$, where -1 , 0 , or 1 represents the CPE as an inductor, resistor, or capacitor, respectively.^{52,53} The pseudocapacitance of a CPE is defined by eq 3:

$$C = (Y_0 R^{1-n})^{1/n} \quad (3)$$

The n values reported in Table 3 were equal to 0.87 without CI with a slight decrease in the presence of PILs (up to 0.81), thus confirming a less heterogeneous surface with respect to the blank and then with less surface damage. The low R_f and C_f values do not show a significant change, which indicates that this parameter does not contribute significantly to the analysis of the PIL anticorrosive properties. The R_L and L values were increased with respect to the blank, which was due to the opposition to the electric current change on the steel surface by means of the adsorption of the species present in the acid–PIL medium and that reflects itself in a higher resistance to the corrosion process of the metal surface.⁵⁴ The EIS polarization resistance (R_{pEIS}) of

the analyzed system was calculated by means of eq 4^{55,56} from the resistive elements conforming the EEC. The R_s values can be neglected due to $R_s \ll R_{ct}$.⁵⁷

$$R_{pEIS} = R_f + \frac{R_{ct}R_L}{R_{ct} + R_L} \quad (4)$$

It is observed that the R_{pEIS} values were increased with C_{INH} , diminishing the charge transfer process and suggesting the protection of the metal surface from the formed PIL film, preventing the acid corrosion process. The IE_{EIS} of the PILs reported in Table 3 are consistent with the IE obtained by the LPR and PDP techniques.

The averaged IE values from the LPR, PDP, and EIS techniques for API 5L X60 steel exposed to 1 M H₂SO₄ and as a function of the concentration of PILs at 25 °C are shown in Figure 6. Based on the obtained results, the IE_{max} values were 76, 81, and 82% in the presence of 175 ppm of poly[VIMC4][Im], poly[VIMC2][Br], and poly[VIMC4][Br], respectively. The PILs show an increase in their IEs from 4 to 10% from 100 to 200 ppm; however, the surface of API 5L X60 steel in the presence of poly[VIMC4][Im] was saturated from 100 ppm; i.e., the surface did not adsorb a higher number of PIL molecules when their concentration was increased, which kept their efficiency without a significant change. The same behavior pattern was observed with poly[VIMC2][Br] and poly[VIMC4][Br] from 175 ppm.

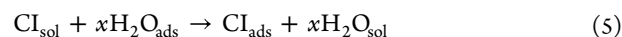
Table 2. Electrochemical Parameters from the LPR and PDP of API 5L X60 Steel in 1 M H₂SO₄–CIs at 25 °C.

CI	C _{INH}	R _p	−β _c	−E _{corr}	i _{corr}	v _{corr}	IE _{LPR}	IE _{PDP}	
	ppm/mM	Ω cm ²	mV dec ^{−1}	mV/Ag/AgCl	μA cm ^{−2}	mm year ^{−1}	%	%	
blank	0/0	35 ± 2	130 ± 3	470 ± 4	548 ± 24	6.36 ± 2.84	-	-	
poly[VIMC4][Im]	25/3.5 × 10 ^{−5}	71 ± 1	124 ± 3	449 ± 2	241 ± 22	2.80 ± 0.25	51 ± 1	56 ± 4	
	50/7.1 × 10 ^{−5}	80 ± 4	127 ± 1	455 ± 1	234 ± 17	2.72 ± 0.20	56 ± 2	57 ± 3	
	75/1.1 × 10 ^{−4}	96 ± 3	142 ± 3	454 ± 1	207 ± 4	2.40 ± 0.05	64 ± 1	62 ± 1	
	100/1.4 × 10 ^{−4}	117 ± 2	141 ± 1	462 ± 1	124 ± 6	1.44 ± 0.07	70 ± 1	77 ± 1	
	125/1.8 × 10 ^{−4}	131 ± 1	133 ± 2	446 ± 1	126 ± 11	1.46 ± 0.13	73 ± 1	77 ± 2	
	150/2.1 × 10 ^{−4}	137 ± 8	136 ± 4	451 ± 1	151 ± 10	1.75 ± 0.12	75 ± 1	72 ± 2	
	175/2.5 × 10 ^{−4}	142 ± 5	135 ± 2	445 ± 1	125 ± 16	1.45 ± 0.19	76 ± 1	77 ± 3	
	200/2.8 × 10 ^{−4}	141 ± 4	141 ± 1	451 ± 1	152 ± 3	1.77 ± 0.03	75 ± 1	72 ± 1	
	poly[VIMC2][Br]	25/4.1 × 10 ^{−5}	59 ± 2	130 ± 2	450 ± 1	301 ± 21	3.50 ± 0.24	41 ± 2	46 ± 4
		50/8.1 × 10 ^{−5}	72 ± 1	126 ± 3	450 ± 1	268 ± 20	3.12 ± 0.23	52 ± 1	51 ± 4
75/1.2 × 10 ^{−4}		91 ± 5	124 ± 1	450 ± 1	193 ± 9	2.24 ± 0.10	62 ± 2	65 ± 2	
100/1.6 × 10 ^{−4}		132 ± 6	125 ± 1	454 ± 1	142 ± 10	1.65 ± 0.11	74 ± 1	74 ± 2	
125/2.0 × 10 ^{−4}		134 ± 10	119 ± 2	454 ± 2	138 ± 15	1.60 ± 0.17	74 ± 2	75 ± 3	
150/2.4 × 10 ^{−4}		143 ± 1	118 ± 1	455 ± 2	121 ± 5	1.41 ± 0.06	76 ± 1	78 ± 1	
175/2.8 × 10 ^{−4}		165 ± 12	121 ± 2	455 ± 1	90 ± 9	1.05 ± 0.11	79 ± 1	84 ± 2	
200/3.3 × 10 ^{−4}		144 ± 18	120 ± 2	450 ± 1	116 ± 13	1.34 ± 0.15	76 ± 3	79 ± 2	
poly[VIMC4][Br]		25/3.5 × 10 ^{−5}	73 ± 1	121 ± 5	453 ± 1	212 ± 24	2.47 ± 0.28	52 ± 1	61 ± 4
		50/7.0 × 10 ^{−5}	98 ± 6	126 ± 2	456 ± 1	190 ± 14	2.21 ± 0.16	64 ± 2	65 ± 2
	75/1.0 × 10 ^{−4}	101 ± 3	128 ± 6	456 ± 2	183 ± 25	2.13 ± 0.29	66 ± 1	67 ± 5	
	100/1.4 × 10 ^{−4}	132 ± 3	137 ± 1	455 ± 1	138 ± 8	1.61 ± 0.10	74 ± 1	75 ± 1	
	125/1.7 × 10 ^{−4}	140 ± 3	121 ± 1	456 ± 2	116 ± 5	1.34 ± 0.06	75 ± 1	79 ± 1	
	150/2.1 × 10 ^{−4}	145 ± 1	123 ± 1	458 ± 1	105 ± 3	1.22 ± 0.04	76 ± 1	81 ± 1	
	175/2.4 × 10 ^{−4}	178 ± 10	118 ± 2	458 ± 2	82 ± 7	0.95 ± 0.09	80 ± 1	85 ± 1	
	200/2.8 × 10 ^{−4}	139 ± 16	115 ± 9	451 ± 1	98 ± 9	1.14 ± 0.10	75 ± 2	82 ± 2	

According to the aforementioned, the corrosion inhibition behavior displayed by the PILs occurred in the following order: poly[VIMC4][Br] > poly[VIMC2][Br] > poly[VIMC4][Im]. This IE trend can be attributed to the adsorption of the different functional groups possessed by each PIL. The IE of poly[VIMC4][Br] is associated with the amount of monomeric units of 1-vinyl-3-butylimidazolium bromide, in addition to having monomers with other functional groups such as vinyl-pyrrolidone and acrylamide, for which, since they possess N and O heteroatoms, a rich electron density that favors adsorption through attraction forces toward the steel surface is provided.⁵⁸ The difference between the IE displayed by poly[VIMC2][Br] and poly[VIMC4][Br] can be related to the length of the alkyl group at N3 of the imidazolium ring that is repeated in block *m*. It has been reported that the electrophilic attack, associated with a loss of electrons, is a function of the length of the alkyl chain: the increase in the alkyl chain in an imidazole ring causes the reactivity with respect to an electrophilic attack to diminish in the imidazole ring but to increase in the alkyl chain.⁵⁹ The extension of the ethyl chain to butyl in the imidazole ring improves the IE because a longer alkyl chain promotes higher electrophilic reactivity in the alkyl chain region, which contributes to the attraction of the PIL toward the steel surface (electron-rich zone).

From the electrochemical results, it can be inferred that the efficiencies of poly[VIMC4][Im] were affected by the low contribution of the diacrylamide block through its N atoms, which could have limited the adsorption of the imidazolium ring, thus provoking a partial protection of the metal surface. The anodic displacements of ΔE_{corr} indicate that the PIL adsorption was promoted mainly by the carbonyl groups and imidazolate ions.

2.2. Adsorption Isotherm. CIs are capable of being adsorbed on a given metal surface to form a protecting film through the replacement of water molecules and/or corrosive ions in the acid medium by CI molecules according to the process shown in eq 5:



The subscripts sol and ads refer to “in solution” and “adsorbed on the surface”, respectively. The coefficient *x* represents the number of water molecules replaced by CI molecules.⁶⁰

The adsorption process of a CI can be explained by means of the adsorption isotherms, which are theoretical mathematical models that can be expressed in terms of the CI molar concentration (C_{INH}) and covered surface degree (θ), which represents the surface fraction protected by the inhibiting action of the PILs. The θ values were calculated with the average of the IE_{LPR}, IE_{PDP}, and IE_{EIS} values from eq 6:

$$\theta = \frac{\text{IE}}{100} \quad (6)$$

In the present work, the Langmuir, Temkin, Frumkin, Freundlich, and Flory–Huggins isotherms were used to fit the PIL experimental data. These mathematical models are shown in Table 4.^{31,61}

The adsorption process of the PILs poly[VIMC4][Im], poly[VIMC2][Br], and poly[VIMC4][Br] on the steel surface obeyed the Langmuir isotherm (Figure 7) whose correlation coefficients (R²) were close to unity (0.992–0.995), as shown in Table 5. This model implies the formation of a CI monolayer on the API 5L X60 steel surface that reduces the active sites.⁶²

The adsorption equilibrium constant (K_{ads}) represents the adsorption–desorption force between the adsorbate (PILs) and adsorbent species (API 5L X60); it shows the equilibrium

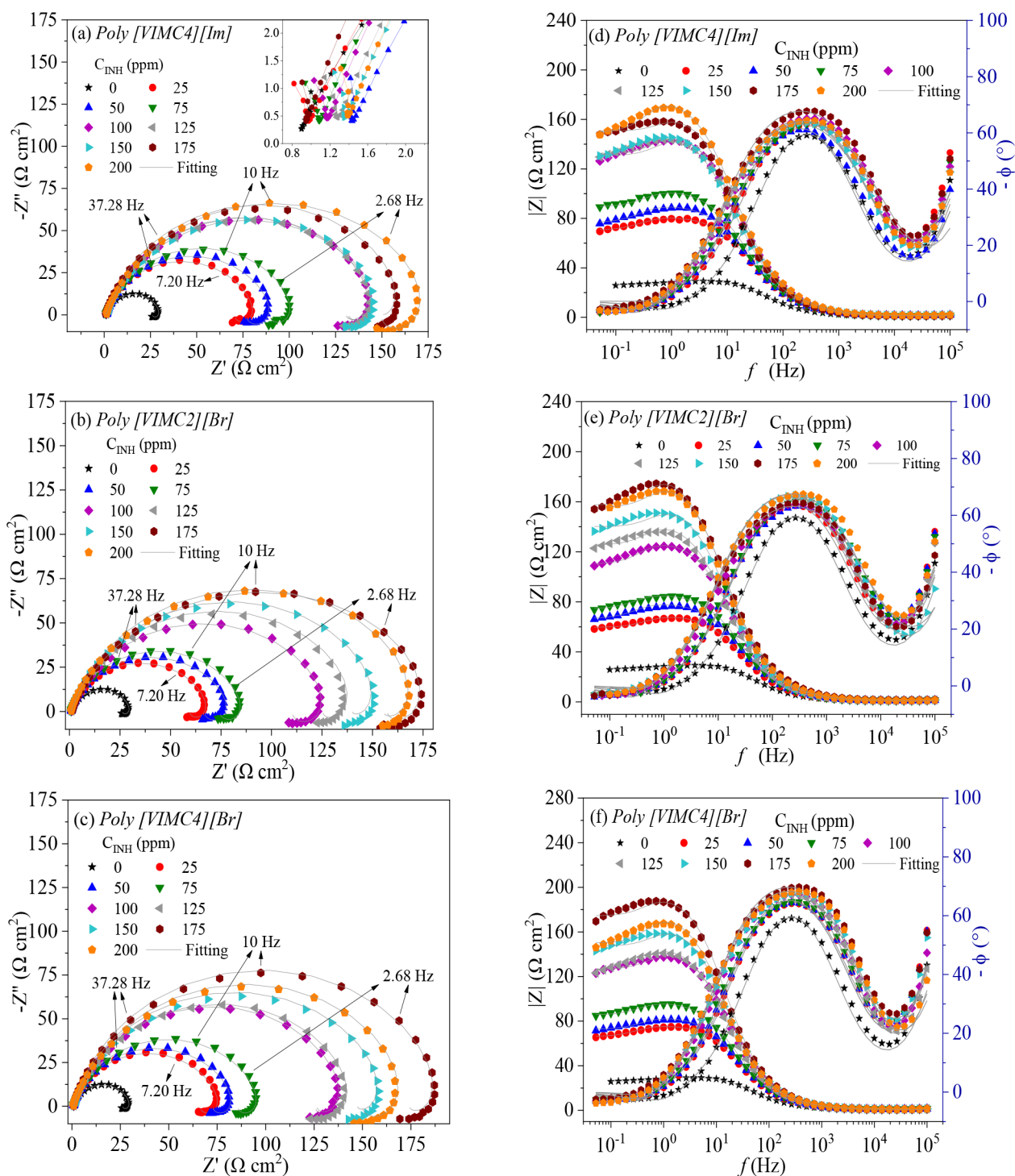


Figure 4. Electrochemical impedance spectra of API SL X60 steel in 1 M H₂SO₄ with and without PILs at 25 °C: (a–c) Nyquist diagram and (d–f) Bode diagram.

relationship between the C_{INH} on the surface and solution core,⁶³ where high K_{ads} values denote improved adsorption efficiency of the CIs.⁶⁴ From Figure 7, the K_{ads} were estimated by the reciprocal of the y -intercept of the linear regression. The K_{ads} of the PILs poly[VIMC4][Im], poly[VIMC2][Br], and poly[VIMC4][Br] adsorbed on the steel surface in 1 M H₂SO₄ at 25 °C are reported in Table 5 with values within the interval ranging from 1.715×10^4 to 3.494×10^4 L mol⁻¹. These values suggest that the PILs were more likely to be adsorbed on the metal surface.⁶⁵

The adsorption process showed by the PILs is described by the standard Gibbs energy of adsorption ($\Delta G_{\text{ads}}^\circ$) whose parameter suggests the adsorption type of the studied metal–liquid system and is defined by eq 7⁶⁶

$$\Delta G_{\text{ads}}^\circ = -RT \ln(55.5K_{\text{ads}}) \quad (7)$$

where R is the ideal gas constant (8.314×10^{-3} kJ mol⁻¹ K⁻¹); T is the absolute temperature in K; and the constant 55.5 represents the water concentration in mol L⁻¹.

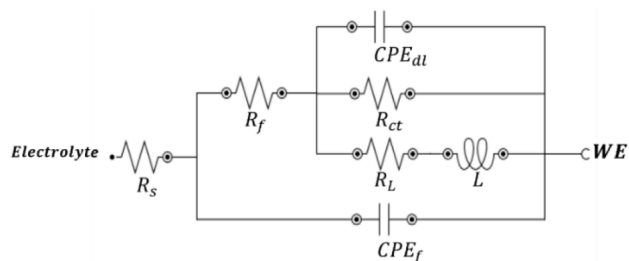


Figure 5. EEC for fitting the EIS experimental data of API SL X60 steel in the presence and absence of CIs at 25 °C.

The literature considers three cases for the thermodynamic parameter $\Delta G^{\circ}_{\text{ads}}$: (i) when it is greater than -20 kJ mol^{-1} , it refers to physical adsorption (physisorption) through electrostatic interactions between the PIL molecules and metal surface; (ii) when it is less than -40 kJ mol^{-1} , it denotes chemical adsorption (chemisorption), which implies the possible formation of a coordinate bond between the PIL and metal surface; and (iii) when it falls between -20 and -40 kJ mol^{-1} , a combined process of physical and chemical adsorption is considered.^{67,68}

Table 5 reports the $\Delta G^{\circ}_{\text{ads}}$ results obtained for the PILs poly[VIMC4][Im], poly[VIMC2][Br], and poly[VIMC4][Br] at 25 °C. The negative values of $\Delta G^{\circ}_{\text{ads}}$ indicate that the adsorption of the CIs was thermodynamically spontaneous⁶⁹ and suggest that a physicochemical adsorption process started through electrostatic forces between the steel surface and N heteroatoms present in the PILs such as vinylpyrrolidone, acrylamide, vinyl alkylimidazolium [VIM⁺] cations, imidazolate [Im⁻] anions, and bromides [Br⁻]. In addition, chemisorption-coordinated complexes can be formed⁷⁰ between the present IL species like vinylalkylimidazolium bromide or vinylbutyl imidazolium imidazolate and the vacant Fe d orbital on the metal surface.

2.3. Surface Analysis. The surface morphology of API SL X60 steel was examined by SEM. Figure 8 shows the micrographs obtained from the blanks in the absence and presence of the PILs after 4 h of immersion at 25 °C. Figure 8(a) presents the attack of the steel surface after being exposed to 1 M H₂SO₄. The microstructure of API SL X60 steel and irregular morphology attributed to severe surface damage by corrosive ions can be observed. Likewise, corrosion products deposited at grain boundaries by the presence of H₃O⁺ and SO₄²⁻ ions in the aqueous medium can be seen.

In contrast, in the presence of CIs (Figures 8b–d), a more homogeneous morphology with less surface damage was obtained. The latter evidences the behavior of poly[VIMC4][Im], poly[VIMC2][Br], and poly[VIMC4][Br] as CIs by the formation of a protecting film on the API SL X60 steel surface, which diminished the ν_{corr} by limiting the migration of corrosive ions and water molecules toward the metal surface.

Table 6 shows the chemical composition and atomic percent obtained by XPS of the API SL X60 steel surface exposed to 1 M H₂SO₄ in the absence and presence of 175 ppm of PILs at 25 °C and 4 h immersion. The elements Fe (2–14 at. %) and O (31–69 at. %) were detected, which indicate the formation of corrosion products such as iron oxides and oxyhydroxides, and the S (3–15 at. %) signals suggest the formation of iron sulfates. The N (2–4 at. %) and C (30–58 at. %) signals confirm the adsorption of the CIs. The O atomic percent is also attributed to the carbonyl groups (C=O) present in the PIL molecules. By

comparing the atomic percentage results of the sample exposed to 1 M H₂SO₄ in the absence and presence of PILs, reported in Table 6, higher percentages of C can be observed for the samples with CIs; furthermore, the absence of N and lower amount of S on the metal surface are the result of the adsorption of poly[VIMC4][Im], poly[VIMC2][Br], and poly[VIMC4][Br] on the steel surface, which blocked the attack of ions in the acid medium.

The high-resolution elemental spectra of O 1s, Fe 2p, N 1s, and C 1s are shown in Figures 9–12. In the O 1s spectrum (Figure 9), the following characteristic peaks are observed: 530.2, 531.8, and 532.9 eV. These peaks are related to oxides, hydrated iron oxides, and iron sulfates, respectively. These corrosion products deposited on the metal surface occurred due to their interaction with O²⁻, OH⁻, and SO₄²⁻ ions.^{71–74} The signal at 532.9 eV also suggests the presence of C=O bonds.⁷⁵ The localized Fe 2p_{3/2} and Fe 2p_{1/2} peaks are shown in Figure 10. The Fe 2p_{3/2} signals were the following: the peak at 711.2 eV characterizes Fe²⁺ (e.g., FeSO₄·H₂O), and the 713.5 and 714.2 eV signals correspond to the satellite peak of ferric compounds Fe³⁺ (e.g., Fe₂O₃, Fe₃O₄, and FeOOH).^{71–73} The Fe 2p_{1/2} signals, which are Fe 2p_{3/2} doublets, were located at 719.2, 724.5, and 727.4 eV. The bond energies of ~ 714 and ~ 727 eV and Fe³⁺ satellite peak at ~ 719 eV confirm the presence of Fe₃O₄.^{76,77} In contrast, the energies of ~ 710 and ~ 724 eV confirm the oxidation of the steel sample, promoting the Fe dissolution. As for the corrosion product film deposited on the metal surface, it was due to the attack of sulfate ions, water molecules, and oxygen due to a postimmersion effect, which was confirmed by the O 1s and Fe 2p spectra.⁷⁸

The N 1s spectrum of the sample evaluated in the presence of PILs (Figure 11) reveals the presence of the $>\text{C}=\text{NH}^+-$ species at 401.6–402.0 eV. These peaks are attributed to the presence of the imidazolium ring of PILs.^{73,75,79} The N–H and/or N–Fe bond(s) detected at 399.9 eV^{74,80–84} is associated with the presence of the amide group of the monomers in the three PILs and/or N–Fe coordination bond(s), respectively. The characteristic C 1s signals of the sample are observed in Figure 12. The peak at 284.8 eV is related to adventitious carbon⁸⁵ and is characteristic of C–C/C–H/C=C bonds,⁷¹ whereas the signal at 286.4 eV is associated with C–O/C–N/C=N bonds.^{72,73,80,86} The C=O bonds were detected with the signal at 288.5 eV.^{86,87} The previous C bonds are related to the monomeric part and polymeric skeleton of the PILs. Based on the signals localized in the N 1s and C 1s spectra, it can be stated that the presence of C and N atoms on the metal surface is related to the bonds present in the imidazolium ring, amide group, and/or imidazolate of the CIs poly[VIMC4][Im], poly[VIMC2][Br], and poly[VIMC4][Br] and suggests that their adsorption process occurred mainly from the N heteroatoms.

2.4. Inhibition Mechanism. The inhibition mechanism of the PILs evaluated on the surface of API SL X60 steel is based on the adsorption phenomenon and was affected by the charge on the metal surface, interaction type with the metal surface, chemical structure, and CI charge distribution.⁸⁸

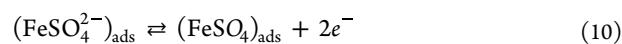


Table 3. Electrochemical Parameters from EIS of API 5L X60 Steel in 1 M H₂SO₄-CIs at 25 °C

CI	C _{NH} ppm/mM	χ^2	R _s		R _t		C _i		R _{ct}		Y ₀		n		C _{dl}		R _L		L		R _{pEIS}		I _{EIS}	
			Ω cm ²	Ω cm ²	μ F cm ⁻²	μ F cm ⁻²	Ω cm ²	Ω cm ²	μ S s ^m cm ⁻²	μ S s ^m cm ⁻²	μ F cm ⁻²	μ F cm ⁻²	Ω cm ²	H cm ²	Ω cm ²	H cm ²	Ω cm ²	Ω cm ²	%	%				
blank	0/0	0.096 ± 0.004	1.57 ± 0.03	2.47 ± 0.04	0.169 ± 0.035	33 ± 3	281 ± 30	0.87	138 ± 10	185 ± 20	31 ± 4	32 ± 3	-											
poly[VIMC4][Br]	25/3.5 × 10 ⁻⁵	0.054 ± 0.001	1.27 ± 0.03	2.24 ± 0.01	0.305 ± 0.004	80 ± 3	234 ± 8	0.83	106 ± 5	440 ± 24	232 ± 7	71 ± 3	55 ± 2											
	50/7.1 × 10 ⁻⁵	0.078 ± 0.011	1.18 ± 0.21	2.34 ± 0.06	0.274 ± 0.010	93 ± 2	225 ± 14	0.83	102 ± 7	540 ± 11	281 ± 3	83 ± 4	61 ± 2											
	75/11.1 × 10 ⁻⁴	0.070 ± 0.022	1.18 ± 0.16	2.28 ± 0.16	0.296 ± 0.037	106 ± 2	223 ± 12	0.83	102 ± 7	650 ± 74	318 ± 1	94 ± 2	66 ± 1											
	100/1.4 × 10 ⁻⁴	0.071 ± 0.007	1.38 ± 0.04	2.49 ± 0.02	0.246 ± 0.002	150 ± 1	192 ± 11	0.82	90 ± 3	867 ± 43	318 ± 1	132 ± 2	76 ± 1											
	125/1.8 × 10 ⁻⁴	0.081 ± 0.017	1.30 ± 0.09	2.52 ± 0.12	0.242 ± 0.008	154 ± 2	196 ± 4	0.82	93 ± 2	895 ± 96	318 ± 1	135 ± 3	76 ± 1											
poly[VIMC2][Br]	150/2.1 × 10 ⁻⁴	0.102 ± 0.004	1.38 ± 0.01	2.69 ± 0.04	0.222 ± 0.004	159 ± 3	209 ± 11	0.81	96 ± 7	852 ± 24	318 ± 1	138 ± 3	77 ± 1											
	175/2.5 × 10 ⁻⁴	0.132 ± 0.013	1.46 ± 0.08	2.33 ± 0.14	0.252 ± 0.027	166 ± 2	187 ± 3	0.84	97 ± 1	1396 ± 11	318 ± 1	152 ± 3	79 ± 2											
	200/2.8 × 10 ⁻⁴	0.103 ± 0.001	2.06 ± 0.01	3.37 ± 0.03	0.146 ± 0.005	186 ± 7	186 ± 1	0.82	88 ± 1	968 ± 12	318 ± 1	161 ± 8	80 ± 1											
	25/4.1 × 10 ⁻⁵	0.072 ± 0.038	1.43 ± 0.02	2.3 ± 0.010	0.286 ± 0.011	66 ± 3	258 ± 9	0.85	122 ± 3	310 ± 59	144 ± 35	58 ± 4	44 ± 4											
	50/8.1 × 10 ⁻⁵	0.084 ± 0.002	1.42 ± 0.00	2.26 ± 0.01	0.278 ± 0.001	77 ± 2	247 ± 7	0.83	112 ± 2	365 ± 21	224 ± 22	68 ± 2	53 ± 1											
poly[VIMC4][Br]	75/1.2 × 10 ⁻⁴	0.111 ± 0.002	1.31 ± 0.04	2.18 ± 0.00	0.280 ± 0.001	86 ± 2	231 ± 13	0.84	109 ± 4	433 ± 46	260 ± 25	75 ± 2	57 ± 1											
	100/1.6 × 10 ⁻⁴	0.074 ± 0.050	1.42 ± 0.16	2.48 ± 0.27	0.254 ± 0.020	127 ± 3	210 ± 15	0.83	104 ± 8	780 ± 14	318 ± 1	113 ± 1	72 ± 2											
	125/2.0 × 10 ⁻⁴	0.117 ± 0.014	1.33 ± 0.01	2.29 ± 0.03	0.268 ± 0.001	144 ± 1	213 ± 6	0.84	108 ± 6	884 ± 2	318 ± 1	127 ± 1	75 ± 1											
	150/2.4 × 10 ⁻⁴	0.109 ± 0.036	2.78 ± 0.58	3.72 ± 0.58	0.228 ± 0.015	159 ± 1	193 ± 5	0.84	102 ± 5	1175 ± 82	318 ± 1	147 ± 1	78 ± 1											
	175/2.8 × 10 ⁻⁴	0.098 ± 0.006	1.34 ± 0.04	2.68 ± 0.02	0.223 ± 0.003	190 ± 1	187 ± 1	0.81	85 ± 2	939 ± 14	318 ± 1	162 ± 1	80 ± 1											
poly[VIMC4][Br]	200/3.3 × 10 ⁻⁴	0.121 ± 0.010	1.49 ± 0.03	2.36 ± 0.05	0.253 ± 0.032	176 ± 3	183 ± 8	0.84	93 ± 5	1231 ± 12	318 ± 1	158 ± 3	80 ± 2											
	25/3.5 × 10 ⁻⁵	0.027 ± 0.006	1.56 ± 0.19	2.42 ± 0.19	0.269 ± 0.037	74 ± 3	239 ± 10	0.84	113 ± 4	401 ± 47	207 ± 36	66 ± 3	52 ± 2											
	50/7.0 × 10 ⁻⁵	0.070 ± 0.016	1.50 ± 0.07	2.39 ± 0.09	0.269 ± 0.008	82 ± 2	228 ± 11	0.84	109 ± 4	454 ± 62	266 ± 63	74 ± 3	56 ± 2											
	75/1.0 × 10 ⁻⁴	0.064 ± 0.005	1.46 ± 0.05	2.38 ± 0.05	0.269 ± 0.007	94 ± 4	226 ± 10	0.84	107 ± 4	547 ± 56	318 ± 1	84 ± 4	62 ± 2											
	100/1.4 × 10 ⁻⁴	0.082 ± 0.032	1.46 ± 0.02	2.5 ± 0.08	0.235 ± 0.016	141 ± 5	191 ± 24	0.83	92 ± 4	875 ± 10	318 ± 1	125 ± 6	74 ± 1											
poly[VIMC4][Br]	125/1.7 × 10 ⁻⁴	0.132 ± 0.013	1.63 ± 0.82	2.58 ± 0.83	0.173 ± 0.114	149 ± 1	200 ± 9	0.84	102 ± 4	837 ± 71	318 ± 1	131 ± 3	76 ± 1											
	150/2.1 × 10 ⁻⁴	0.110 ± 0.014	1.54 ± 0.15	2.47 ± 0.14	0.242 ± 0.017	171 ± 8	176 ± 7	0.84	90 ± 4	1083 ± 16	318 ± 1	151 ± 9	79 ± 1											
	175/2.4 × 10 ⁻⁴	0.115 ± 0.006	1.99 ± 0.92	3.03 ± 0.58	0.174 ± 0.076	196 ± 1	162 ± 20	0.83	81 ± 2	1228 ± 14	318 ± 1	174 ± 2	82 ± 2											
	200/2.8 × 10 ⁻⁴	0.150 ± 0.029	2.08 ± 0.58	2.87 ± 0.57	0.121 ± 0.032	169 ± 10	186 ± 12	0.84	95 ± 5	879 ± 38	318 ± 1	147 ± 8	78 ± 1											

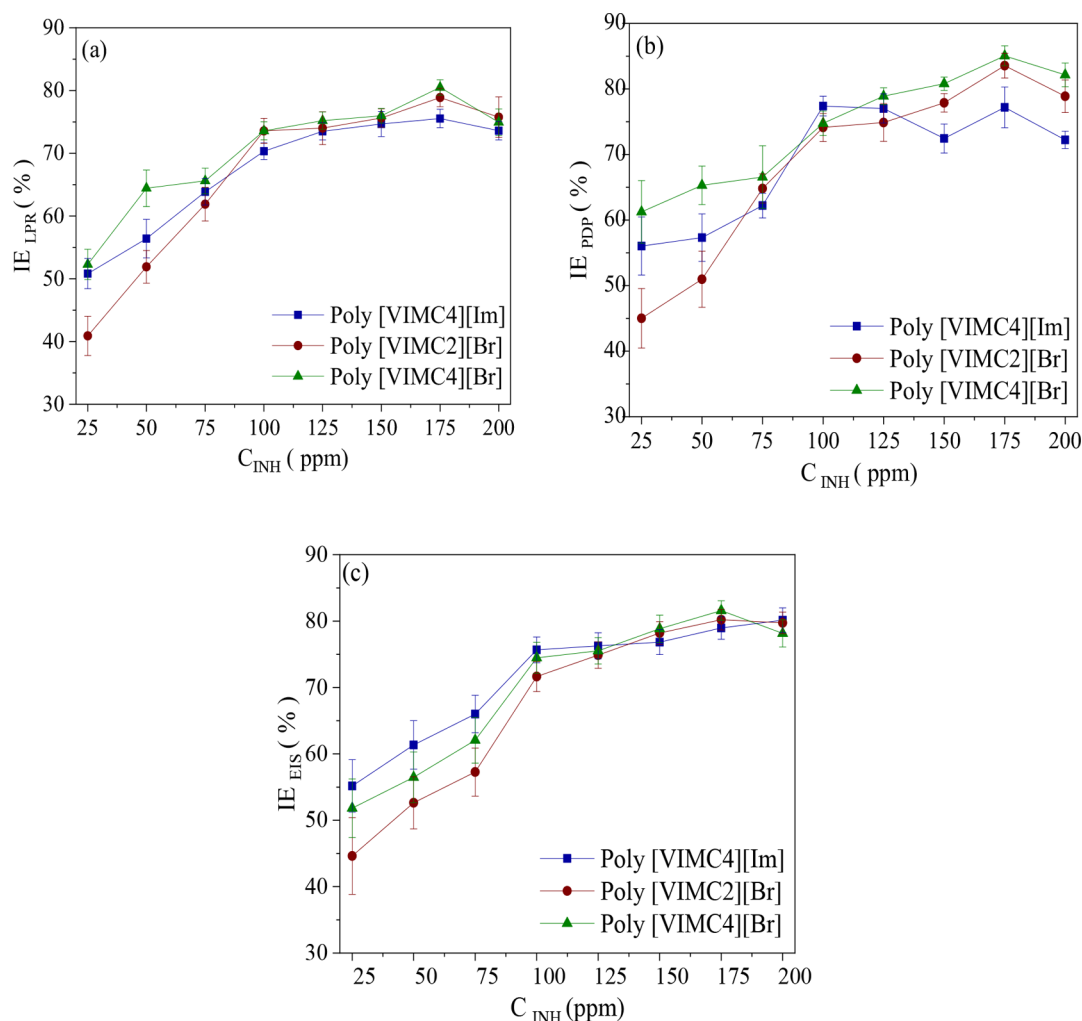
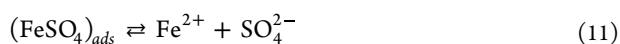


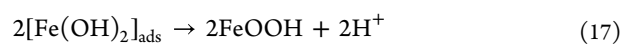
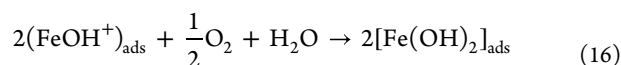
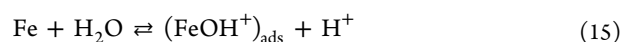
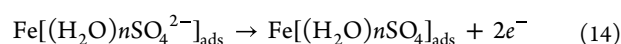
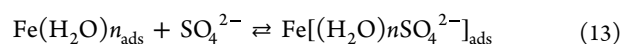
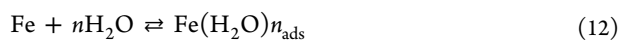
Figure 6. Inhibition efficiency for API 5L X60 steel in 1 M H₂SO₄ in the absence and presence of CIs at 25 °C employing the (a) LPR, (b) PDP, and (c) EIS techniques.

Table 4. Models of Adsorption Isotherms Used to Evaluate CIs

isotherm	nonlinear model	linear model	plot (y vs x)
Langmuir	$K_{\text{ads}}C_{\text{inh}} = \frac{\theta}{\theta - 1}$	$\frac{C_{\text{inh}}}{\theta} = C_{\text{inh}} + \frac{1K}{K_{\text{ads}}}$	$\frac{C_{\text{inh}}}{\theta}$ vs C_{inh}
Temkin	$K_{\text{ads}}C_{\text{inh}} = e^{f\theta}$	$f\theta = \ln C_{\text{inh}} + \ln K_{\text{ads}}; f = -2a$	θ vs $\ln C_{\text{inh}}$
Frumkin	$K_{\text{ads}}C_{\text{inh}} = \left(\frac{\theta}{1-\theta}\right)e^{f\theta}$	$f\theta = \ln\left[\frac{\theta}{(1-\theta)C_{\text{inh}}}\right] + \ln K_{\text{ads}}$	θ vs $\ln\left[\frac{\theta}{(1-\theta)C_{\text{inh}}}\right]$
Freundlich	$K_{\text{ads}}C_{\text{inh}} = \theta$	$\ln \theta = \ln C_{\text{inh}} + \ln K_{\text{ads}}$	$\ln \theta$ vs $\ln C_{\text{inh}}$
Flory–Huggins	$\frac{\theta}{C_{\text{inh}}} = K_{\text{ads}}(1 - \theta)^n$	$\ln\left(\frac{\theta}{C_{\text{inh}}}\right) = \ln K_{\text{ads}} + n \ln(1 - \theta)$	$\ln\left(\frac{\theta}{C_{\text{inh}}}\right)$ vs $\ln(1 - \theta)$



The negatively charged SO_4^{2-} ion was adsorbed easily on the anodic sites of the positively charged metal surface,⁸⁹ which favored the surface passivation by means of the formed iron sulfates (eqs 9 and 10); however, iron dissolution (eq 11) and other reactions that promoted the formation of other corrosion products such as hydrated iron sulfates (rozenite and melanterite) (eqs 12–14),⁹⁰ iron oxides (II and III), or iron oxyhydroxides like akaganeite, lepidocrocite, and/or goethite (eqs 15–17) also took place:³⁵



The ΔE_{corr} with anodic preference indicates that the metal surface can be inhibited by the PIL cations through a negatively charged intermediate like imidazolate $[\text{Im}^-]$ and bromide $[\text{Br}^-]$

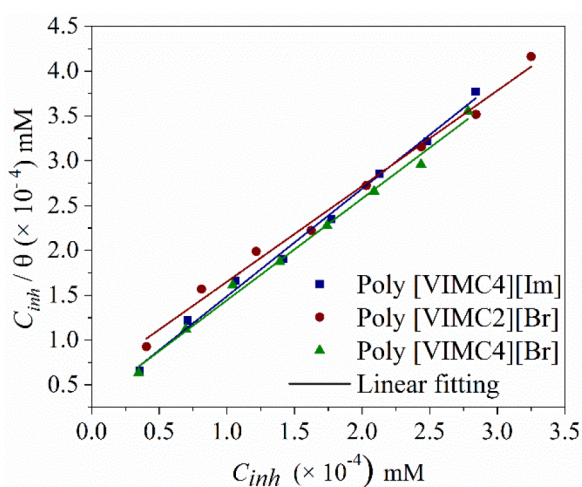
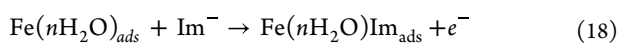


Figure 7. Langmuir adsorption isotherm of API 5L X60 steel in 1 M H_2SO_4 with CIs at 25 °C.

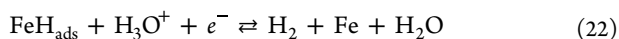
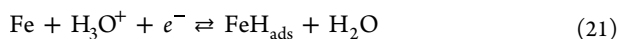
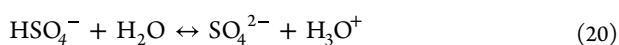
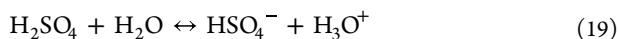
Table 5. Thermodynamic Parameters from the Langmuir Adsorption Isotherms of CIs at 25 °C

PIL	R^2	slope	$K_{\text{ads}}(\text{L mol}^{-1})$	$-\Delta G_{\text{ads}}^\circ$ (kJ mol^{-1})
poly[VIMC4][Im]	0.995	1.201	3.494×10^4	35.88
poly[VIMC2][Br]	0.992	1.221	1.715×10^4	34.12
poly[VIMC4][Br]	0.994	1.112	3.233×10^4	35.69

and/or SO_4^{2-} anions present in solution (eq 18),⁶³ which occupy the surface active sites and then diminish the iron dissolution reaction (eq 8). The latter suggests that the inhibitor can be adsorbed physically by Coulombic attraction between PIL molecules and the steel surface.⁹¹ The $[\text{Im}^-]$ anion, like most organic anions, occupies larger geometric space in comparison with $[\text{Br}^-]$, which improves the covering of anodic sites. Notwithstanding, the anticorrosive property of PILs is the result of the effect exerted by the cation and anion on the general corrosion process:

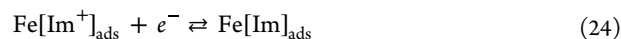


In contrast, the hydronium ions (H_3O^+), formed during eqs 19 and 20, are attracted to the cathodic zone,⁹² where their reduction and further formation of molecular hydrogen occur (eqs 21 and 22); the freed electrons are used in the anodic reactions:⁹³



Since PILs possess a positive charge, they are adsorbed on the cathodic sites by means of the alkylimidazolium unit, where the $[\text{Im}^+]$ cations of PILs, in addition to having π electrons in their aromatic imidazolium ring, present bigger size and higher electron density with respect to protons (H^+), thus promoting a competition among them. In the cathodic sites, the adsorption of CIs is eased by van der Waals forces, occupying higher surface area and forming a barrier that prevents the attack of corrosive ions.⁹⁴ Physisorption is the main process occurring (eq 23);

however, chemical adsorption also takes place with the possible formation of iron–PIL complexes (eq 24) according to the obtained $\Delta G_{\text{ads}}^\circ$ data:



The polymeric chain of PILs works as a physical barrier that limits the passing of water and aggressive ions.^{95–97} By comparing the results obtained from the electrochemical tests of the PILs poly[VIMC4][Br] and poly[VIMC4][Im], it can be concluded that poly[VIMC4][Br] displayed better anticorrosive performance than poly[VIMC4][Im] because the first one has a straight structure whereas the second one is a reticulated polymer due to the bisacrylamide methylene bridges that are linked to the polymeric chains, forming a network. Poly[VIMC2][Br] has a lateral ethyl alkyl chain, two carbon atoms shorter than butyl, which affected its capacity to repel water from the metal surface, producing slightly lower IEs than poly[VIMC4][Br].

In contrast, even with the presence of the imidazolate anion, which has π electrons and can form chemical bonds with iron, the accommodation of poly[VIMC4][Im] on the metal surface became difficult due to its reticulated polymeric chain; however, the linear chain of poly[VIMC4][Br] suggests that it was adsorbed with higher order on the metal surface. The result of the synergistic effect of the anion and cation indicates that the properties of poly[VIMC4][Br] and poly[VIMC4][Im] were very similar.

Figure 13 shows that the inhibition mechanism of the PILs occurred through the adsorption process promoted by the electrostatic interaction and limited by diffusion. First, the CI molecules diffused from the solution core toward the interphase layer of the metal surface under a C_{INH} gradient. Afterward, they joined the charged metal substrate by electrostatic attraction of the acrylamide, vinylpyrrolidone, and vinylalkylimidazolium polymeric units, anchoring on the surface, forming loops and a train of segments adhered to tails protruding toward the solution core. The electrostatic attraction drove to the spatial reorganization of the polymeric skeleton of the PILs due to the higher contact with the API 5L X60 steel and to a more extended configuration, parallel to the metal surface,⁹⁸ forming a CI monolayer in C_{dl} through the N, C, and O atoms present in the PILs as shown by the high-resolution XPS spectra.

3. CONCLUSIONS

The present research work dealt with the IE evaluation of three PILs synthesized to prevent API 5L X60 steel from being corroded in an acidic medium. In addition to the IE, adsorption properties on the metallic surface were studied by means of electrochemical and surface analysis techniques. As a result, all the PILs were classified as mixed-type CIs, and poly[VIMC4]-[Br] was identified as the most promising CI with an IE of 85%. Due to their chemical structure, these compounds protected the steel material through their physicochemical adsorption. These results correlated well with the surface analyses employed in this study. In general, from the results reported in the present research work, it can be concluded that CIs of the PIL type represent a feasible strategy to inhibit the corrosion of steel elements omnipresent in the oil industry when the properties of repeating units (monomers) and specific features of anion structures are combined suitably in this type of compound.

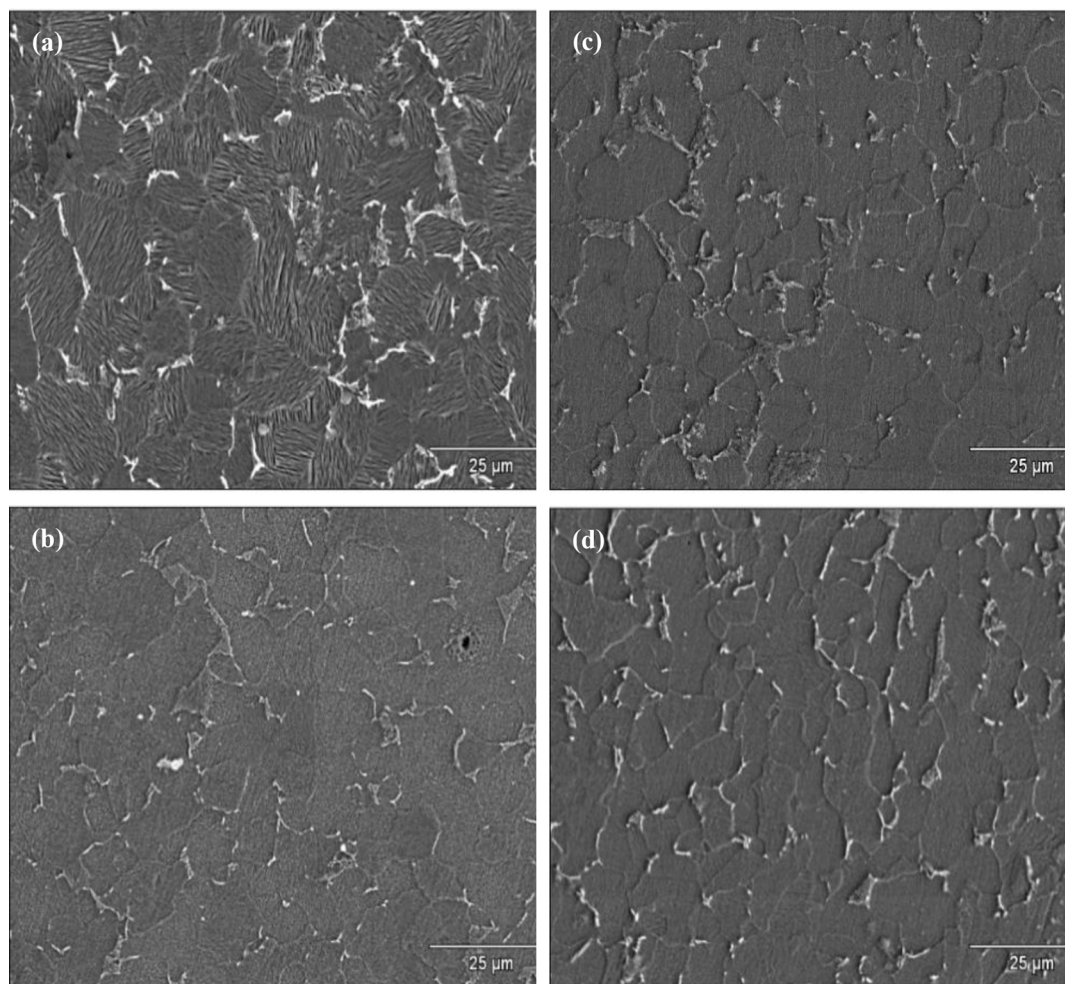


Figure 8. SEM images of API 5L X60 steel after immersion for 4 h in 1 M H₂SO₄ and 175 ppm of PILs: (a) blank, (b) poly[VIMC4][Im], (c) poly[VIMC2][Br], and (d) poly[VIMC4][Br].

Table 6. Chemical Composition Obtained by XPS from the API 5L X60 Steel Surface after 4 h of Immersion in 1M H₂SO₄ in the Presence of PILs

sample	chemical composition (at. %)				
	Fe 2p	O 1s	S 2p	N 1s	C 1s
blank	6.48	68.52	15.48	-	9.52
poly[VIMC4][Im]	2.71	31.20	3.41	4.34	58.34
poly[VIMC2][Br]	8.66	46.25	3.50	4.09	37.50
poly[VIMC4][Br]	14.22	48.65	4.46	2.00	30.67

4. EXPERIMENTAL SECTION

4.1. Materials and Equipment. The reagents 1-vinylimidazole (VIM, $\geq 99\%$), bromoethane (99%), and 1-bromobutane (99%) were used to obtain 1-vinyl-3-ethylimidazole bromide ([VIMC2][Br]) and 1-vinyl-3-butylimidazole bromide ([VIMC4][Br]) monomers. *N*-Vinyl-2-pyrrolidone (VP, $\geq 99\%$) and acrylamide (AM, $\geq 98\%$) were used as comonomers. *N,N'*-Methylenebis(acrylamide) (BAM, 99%) was used as a cross-linking agent, and 2,2'-azobis(2-methylpropionamide) dihydrochloride (V50, 97%) was used as the polymerization initiator. All reagents were purchased from Sigma-Aldrich. High purity nitrogen gas (99.9%) was used for degassing mixtures of reaction solutions and was purchased from Praxair. ¹H NMR (300 MHz) spectra were obtained with a Jeol

Eclipse-300 equipment using tetramethylsilane (TMS) as the internal standard and deuterated water or methanol as solvent at room temperature. Infrared spectra were obtained on a Nicolet Nexus 470 FT-IR spectrometer in attenuated total reflection (ATR) mode. Molecular weights were measured in a GPC Agilent series 1260 Infinity equipment with 2 Aquagel-OH Mixed-H 8 $\mu\text{m} \times 7.5$ mm columns connected in series.

The thermal properties of PILs were determined by high-resolution thermogravimetric analysis (TGA) using a Netzsch STA 409 in a nitrogen atmosphere at temperatures ranging from 30 to 600 °C (rate 5 °C/min).

4.2. Polymer Synthesis. [VIMC4][Br] and [VIMC2][Br] monomers were obtained by following a previously described procedure.^{99,100} Poly[VIMC4][Im] was synthesized through a previously reported procedure,²⁷ using 0.02 mol % of BAM per mole of monomer in the initial reaction mixture (see Figure 14). Bisacrylamide (BAM) is used as an organic cross-linker to form cross-linked polymers, which increases the viscosity by forming a three-dimensional network.

The terpolymers poly[VIMC2][Br] and poly[VIMC4][Br] were prepared from AM, VP, and [VIMC2][Br] or [VIMC4][Br] following the same procedure (see Figure 15). The molar ratio in the initial reaction mixture was (35–35–30), respectively. To obtain the terpolymer poly[VIMC4][Br], 1.94 g (27.3 mmol) of AM, 3.04 g (27.3 mmol) of VP, and 5.42 g (23.4 mmol) of [VIMC4][Br] were added to 40 mL of

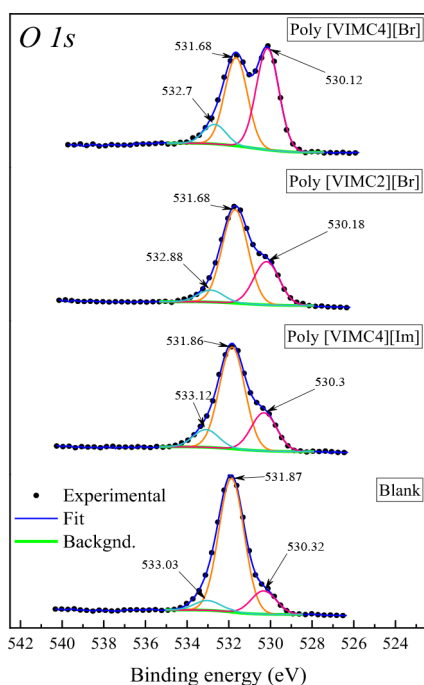


Figure 9. High-resolution XPS spectra of O 1s of API SL X60 steel in the presence of CIs at 25 °C and 4 h immersion.

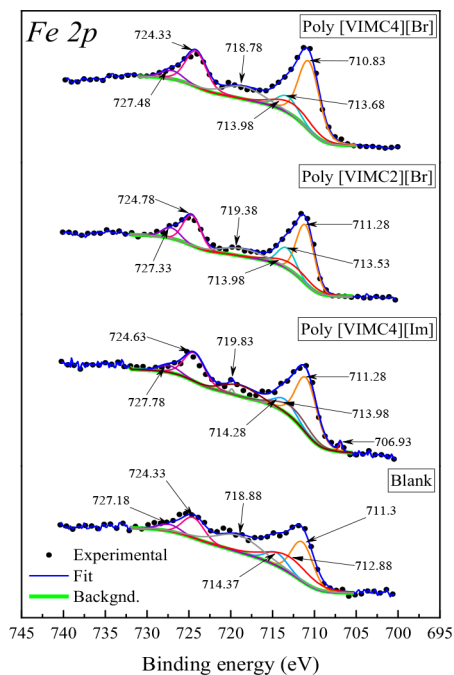


Figure 10. High-resolution XPS spectra of Fe 2p of API SL X60 steel in the presence of CIs at 25 °C and 4 h immersion.

deionized water in a three-neck round-bottom flask equipped with a mechanical stirrer (80 rpm). The reaction solution was cooled to 3 °C and degassed by vacuum for 15 min, and then it was returned to ambient pressure by circulating nitrogen in the system. Once the system reached the reaction temperature of 50 °C, 0.148 g (0.546 mmol) of the initiator V50 diluted in deionized and degassed water was pumped into the reaction mixture for 30 min. The reaction was allowed to continue with a constant flow of nitrogen for 8 h. The initiator concentration in the reaction was 0.007 mol of initiator per mole of monomers.

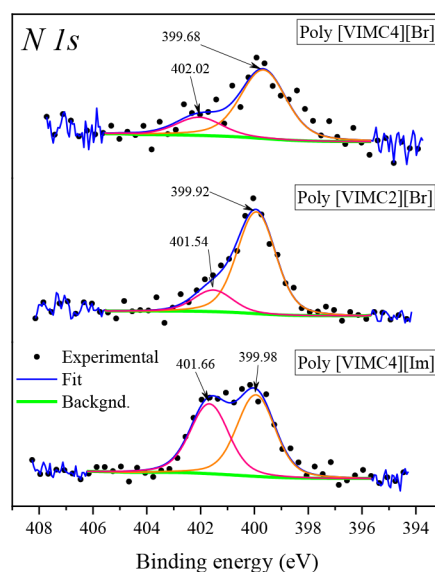


Figure 11. High-resolution XPS spectra of N 1s of API SL X60 steel in the presence of CIs at 25 °C and 4 h immersion.

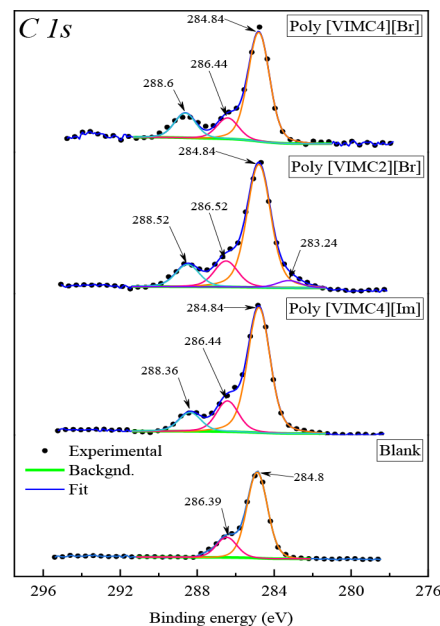


Figure 12. High-resolution XPS spectra of C 1s of API SL X60 steel in the presence of CIs at 25 °C and 4 h immersion.

The terpolymer was separated from the reaction mixture by precipitation in acetone and dried at 40 °C under vacuum for 24 h.

The molecular weights of the polymers evaluated as CIs are 702 314, 823 530 and 884 350 g mol⁻¹ for poly[VIMC4][Im], poly[VIMC2][Br], and poly[VIMC4][Br], respectively. The displacements obtained by ¹H NMR and FTIR are the following (Figures S1–S3, Supporting Information).

Poly(1-butyl-3-vinylimidazolium) imidazolate, Poly-[VIMC4][Im]. ¹H NMR (MeOD, 300 MHz) δ_{H} (ppm): 1.03 (b, 3H), 1.43 (b, 2H), 1.91 (b, 2H), 2.68 (b, 2H), 4.24 (b, 2H), 6.95 (s, 2H), 7.12 (s, 1H), 7.68 (s, 2H), 8.53 (s, 1H). FT-IR (500–4000 cm⁻¹, ATR): ν 3172, 2962, 2881, 1556, 1473, 1168, 839, 557.

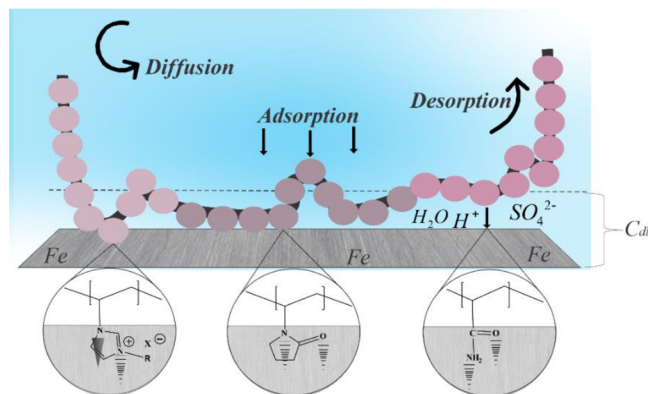


Figure 13. Inhibition mechanism of PILs on API SL X60 steel in 1 M H_2SO_4 at 25 °C.

Poly(acrylamide-N-vinylpyrrolidone-1-ethyl-3-vinylimidazolium bromide), poly[VIMC2][Br]. ^1H NMR (D_2O , 300 MHz) δ_{H} (ppm): 1.2–2.69 (b, 14H), 3.27 (b, 2H), 4.02 (b, 2H), 4.24 (b, 2H), 7.61 (b, 3H). FT-IR (500–4000 cm^{-1} , ATR): 3353, 3187, 2917, 1646, 1438, 1290, 1160.

Poly(acrylamide-N-vinylpyrrolidone-1-butyl-3-vinylimidazolium bromide), Poly[VIMC4][Br]. ^1H NMR (D_2O , 300 MHz) δ_{H} (ppm): 0.96 (b, 3H), 1.36 (b, 2H), 1.44–2.68 (b, 13H), 3.26 (b, 2H), 3.27 (2H), 3.9 (b, 2H), 4.2 (b, 2H), 7.62 (b, 3H). FT-IR (500–4000 cm^{-1} , ATR): ν 3358, 3179, 2916, 1645, 1436, 1290, 1162. Additionally, Figure S4 (Supporting Information) shows the thermograms obtained for the PILs. The first weight loss stage corresponded to water loss, which occurred between 30 and 120 °C and was of 7, 10, and 14% for poly[VIM4][IM], poly[VIM4C][Br], and poly[VIM2C][Br], respectively. The homopolymer poly[VIM4][IM] was decomposed in a single weight loss stage, which started at 247 °C. In contrast, the decomposition of the terpolymers poly[VIM4C][Br] and poly[VIM2C][Br] took place in two clearly defined stages at 245 and 250 °C, respectively. The first stage was ascribed to the decomposition of side acrylamide groups by the elimination of

ammonia, forming imide groups;^{101,102} at this stage, the decomposition of repeating PIL units is also found.^{103,104} The second stage was related to the decomposition of the repeating units of *n*-vinylpyrrolidone.

4.3. Preparation of Steel Specimens and Acid Medium.

For the evaluation of the PILs as CIs in an acid medium, the working electrodes (WEs) were previously prepared using API 5L X60 steel samples with the following chemical composition: C (0.14%), Mn (1.04%), Si (0.25%), Cr (0.07%), Mo (0.08%), V (0.03%), Cu (0.03%), Ni (0.05%), Al (0.026%), P (0.014%), S (0.011%), Ti (0.015%), Nb (0.001%), and Fe (balance).¹⁰⁵ The WE had exposed surface areas of 0.2894 cm^2 . Before each experiment, such a surface was abraded with SiC sheets with grades from 600 to 1200; afterward, the material was rinsed with distilled water and ethanol, drying it with nitrogen at ambient temperature.¹⁰⁶ The corrosive medium of 1 M H_2SO_4 (blank) was prepared by mixing analytic grade H_2SO_4 and deionized water. The water-soluble PILs were evaluated at concentrations ranging from 25 to 200 ppm in the corrosive medium.

4.4. Electrochemical Measurements. The electrochemical analyses were carried out by means of a potentiostat/galvanostat instrument model Metrohm Autolab PGSTAT 302N controlled by the software NOVA 2.1.4. The H_2SO_4 –PIL system was analyzed in a glass cell equipped with three electrodes: a Ag/AgCl electrode employed as a reference electrode (RE), a Pt electrode used as a counter electrode (CE), and the WE. The open-circuit potential (E_{OCP}) was established after immersing the WE in the corrosive solution with and without CI for 20 min. The employed electrochemical techniques were the following: LPR within a ± 25 mV interval and PDP within a ± 250 mV interval, both at a rate of 0.1666 mV s^{-1} . The EIS was performed within a frequency interval ranging from 100 kHz to 100 mHz with a sinusoidal wave featuring 5.0 mV of amplitude.¹⁰⁷ All the electrochemical tests were done in triplicate with respect to the E_{OCP} at 25 ± 1 °C.^{106–109} The inhibition efficiency (IE) of the PILs was calculated from the obtained LPR, PDP, and EIS results, employing eqs 25 and 26^{5,90}

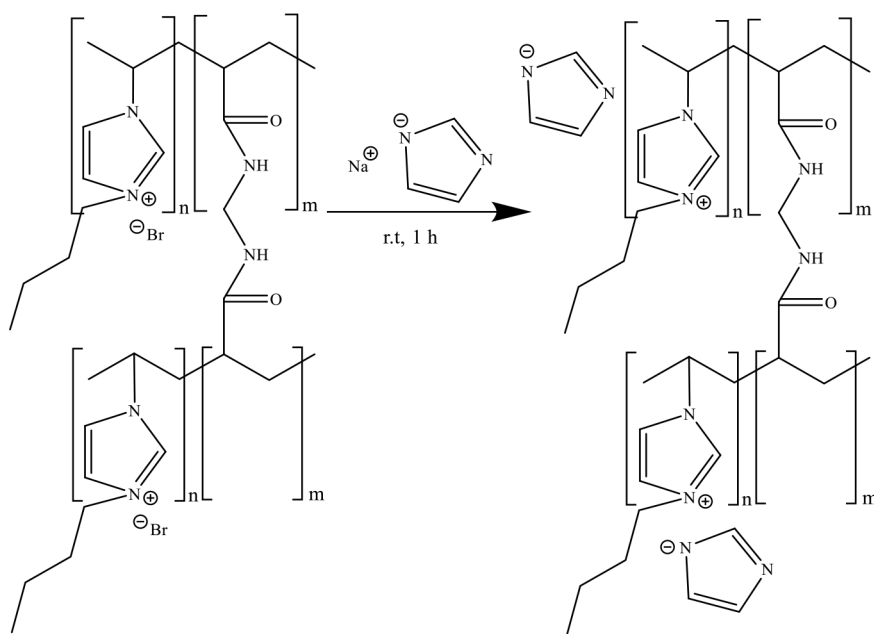


Figure 14. Schematic representation of the ion exchange reaction to obtain cross-linked poly[VIMC4][Im].

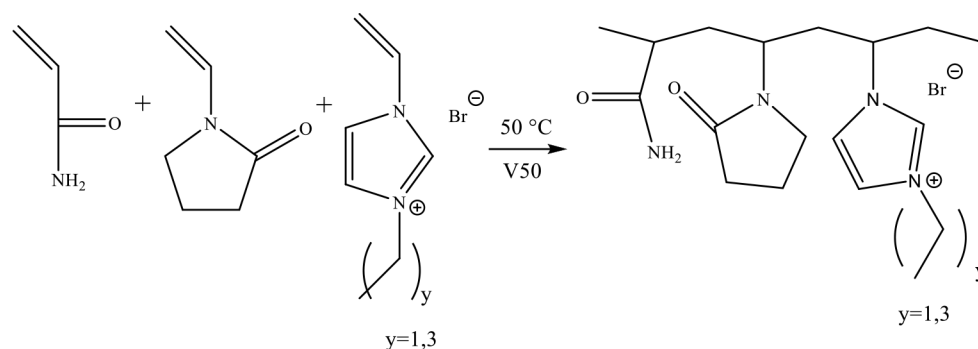


Figure 15. Polymerization reaction for obtaining poly[VIMC2][Br] ($y = 1$) and poly[VIMC4][Br] ($y = 3$).

$$IE_{\text{LPR,EIS}} = \left[\frac{R_p^{\text{Cl}} - R_p^0}{R_p^{\text{Cl}}} \right] \times 100 \quad (25)$$

$$IE_{\text{PDP}} = \left[\frac{i_{\text{corr}}^0 - i_{\text{corr}}^{\text{Cl}}}{i_{\text{corr}}^0} \right] \times 100 \quad (26)$$

where R_p is the polarization resistance obtained by either the LPR or EIS technique expressed in $\Omega \text{ cm}^2$; i_{corr} is the current density in $\mu\text{A cm}^{-2}$; and the Cl and 0 superindices denote the presence and absence of PILs in the acid system, respectively.

4.5. Surface Analysis. The surfaces of the API 5L X60 steel samples were analyzed through the SEM and XPS techniques. The steel samples were immersed in 1 M H_2SO_4 in the absence and presence of 175 ppm of CIs for 4 h.^{106,110} The surface morphology was analyzed employing a scanning electron microscope model JEOL-JSM-6300. The XPS analysis was performed by means of an ESCALAB spectrometer by VG Scientific with an Al K α X-ray monochromatic source of 1486.6 eV. The analyzer pass energy was of 20 eV. The obtained spectra were referred to as adventitious carbon (284.8 eV), and the peak fitting was done using the software Thermo Avantage v.5.9915.

■ ASSOCIATED CONTENT

SI Supporting Information

The Supporting Information is available free of charge at <https://pubs.acs.org/doi/10.1021/acsomega.2c04787>.

Figure S1: ¹H NMR of poly(1-butyl-3-vinylimidazolium) imidazololate. Figure S2: ¹H NMR of (a) poly(acrylamide-*N*-vinylpyrrolidone-1-ethyl-3-vinylimidazolium [bromide]), poly[VIMC2][Br], and (b) poly(acrylamide-*co-N*-vinylpyrrolidone-*co*-1-butyl-3-vinylimidazolium [bromide]), poly[VIMC4][Br]. Figure S3: FTIR of (a) poly[VIMC2][Br], (b) poly[VIMC4][Br], and (c) poly[VIMC4][Im]. Figure S4: TGA curves of poly(ionic liquids) used in the study (PDF)

■ AUTHOR INFORMATION

Corresponding Authors

Paulina Arellanes-Lozada – Benemérita Universidad Autónoma de Puebla, Facultad de Ingeniería Química, C. P. 72570 Puebla, Puebla, México; orcid.org/0000-0003-0918-5008; Email: paulina.arellanes@correo.buap.mx

Octavio Olivares-Xometl – Benemérita Universidad Autónoma de Puebla, Facultad de Ingeniería Química, C. P. 72570 Puebla, Puebla, México; orcid.org/0000-0003-0525-6155; Email: octavio.olivares@correo.buap.mx

Authors

Giselle Gómez-Sánchez – Benemérita Universidad Autónoma de Puebla, Facultad de Ingeniería Química, C. P. 72570 Puebla, Puebla, México; orcid.org/0000-0002-5119-5501

Natalya V. Likhanova – Instituto Mexicano del Petróleo, Gerencia de Materiales y Desarrollo de Productos Químicos, C. P. 07730 Ciudad de México, CDMX, México; orcid.org/0000-0003-4152-0953

Irina V. Lijanova – Instituto Politécnico Nacional, CIITEC, Cerrada Cecati S/N, C. P. 02250 Ciudad de México, CDMX, México

Víctor Díaz-Jiménez – Benemérita Universidad Autónoma de Puebla, Facultad de Ingeniería Química, C. P. 72570 Puebla, Puebla, México; orcid.org/0000-0001-8730-4717

Diego Guzmán-Lucero – Instituto Mexicano del Petróleo, Gerencia de Materiales y Desarrollo de Productos Químicos, C. P. 07730 Ciudad de México, CDMX, México; orcid.org/0000-0001-8113-7364

Janette Arriola-Morales – Benemérita Universidad Autónoma de Puebla, Facultad de Ingeniería Química, C. P. 72570 Puebla, Puebla, México; orcid.org/0000-0002-4745-5868

Complete contact information is available at:

<https://pubs.acs.org/doi/10.1021/acsomega.2c04787>

Notes

The authors declare no competing financial interest.

■ ACKNOWLEDGMENTS

Gómez-Sánchez acknowledges CONACYT for the scholarship granted to pursue postgraduate studies. G.G.S., P.A.L., O.O.X., V.D.J., and J.A.M. thank the support provided by BUAP-FIQ and VIEP to carry out the present project.

■ REFERENCES

- Allahkaram, S. R.; Isakhani-Zakaria, M.; Derakhshani, M.; Samadian, M.; Sharifi-Rasaey, H.; Razmjoo, A. Investigation on corrosion rate and a novel corrosion criterion for gas pipelines affected by dynamic stray current. *J. Nat. Gas Sci. Eng.* **2015**, *26*, 453–460.
- Sastri, V. S. Consequences of Corrosion. In *Challenges in Corrosion: Costs, Causes, Consequences, and Control*; John Wiley & Sons, 2015; pp 317–402.
- Farhadian, A.; Rahimi, A.; Safaei, N.; Shaabani, A.; Abdouss, M.; Alavi, A. A theoretical and experimental study of castor oil-based inhibitor for corrosion inhibition of mild steel in acidic medium at elevated temperatures. *Corros. Sci.* **2020**, *175*, 108871.
- Yesudass, S.; Olasunkanmi, L. O.; Bahadur, I.; Kabanda, M. M.; Obot, I. B.; Ebenso, E. E. Experimental and theoretical studies on some selected ionic liquids with different cations/anions as corrosion

- inhibitors for mild steel in acidic medium. *J. Taiwan Inst. Chem. Eng.* **2016**, *64*, 252–268.
- (5) Sastri, V. S.; Ghali, E.; Elboudjaini, M. Corrosion Testing, Detection, Monitoring and Failure Analysis. In *Corrosion Prevention and Protection: Practical Solutions*, 1st ed.; John Wiley & Sons, 2007; pp 109–176.
- (6) Machado Fernandes, C.; Faro, L. V.; Pina, V. G. S. S.; de Souza, M. C. B. V.; Boechat, F. C. S.; de Souza, M. C.; Briganti, M.; Totti, F.; Ponzio, E. A. Study of three new halogenated oxoquinolinecarbohydrazide N-phosphonate derivatives as corrosion inhibitor for mild steel in acid environment. *Surf. Interfaces* **2020**, *21*, 100773.
- (7) Feng, L.; Zhang, S.; Qiang, Y.; Xu, S.; Tan, B.; Chen, S. The synergistic corrosion inhibition study of different chain lengths ionic liquids as green inhibitors for X70 steel in acidic medium. *Mater. Chem. Phys.* **2018**, *215*, 229–241.
- (8) Boulhaoua, M.; El Hafi, M.; Zehra, S.; Eddaif, L.; Alrashdi, A. A.; Lahmidi, S.; Guo, L.; Mague, J. T.; Lgaz, H. Synthesis, structural analysis and corrosion inhibition application of a new indazole derivative on mild steel surface in acidic media complemented with DFT and MD studies. *Colloids Surf., A* **2021**, *617*, 126373.
- (9) Murmu, M.; Saha, S. K.; Bhaumick, P.; Murmu, N. C.; Hirani, H.; Banerjee, P. Corrosion inhibition property of azomethine functionalized triazole derivatives in 1 mol L⁻¹ HCl medium for mild steel: Experimental and theoretical exploration. *J. Mol. Liq.* **2020**, *313*, 113508.
- (10) Saha, S. K.; Dutta, A.; Ghosh, P.; Sukul, D.; Banerjee, P. Novel Schiff-base molecules as efficient corrosion inhibitors for mild steel surface in 1 M HCl medium: experimental and theoretical approach. *Phys. Chem. Chem. Phys.* **2016**, *18* (27), 17898–17911.
- (11) Sengupta, S.; Murmu, M.; Mandal, S.; Hirani, H.; Banerjee, P. Competitive corrosion inhibition performance of alkyl/acyl substituted 2-(2-hydroxybenzylideneamino)phenol protecting mild steel used in adverse acidic medium: A dual approach analysis using FMOs/molecular dynamics simulation corroborated experimental findings. *Colloids Surf., A* **2021**, *617*, 126314.
- (12) Sarkar, T. K.; Saraswat, V.; Mitra, R. K.; Obot, I. B.; Yadav, M. Mitigation of corrosion in petroleum oil well/tubing steel using pyrimidines as efficient corrosion inhibitor: Experimental and theoretical investigation. *Mater. Today Commun.* **2021**, *26*, 101862.
- (13) Ajjan, F. N.; Ambrogi, M.; Tiruye, G. A.; Cordella, D.; Fernandes, A. M.; Grygiel, K.; Isik, M.; Patil, N.; Porcarelli, L.; Rocasalbas, G.; et al. Innovative polyelectrolytes/poly(ionic liquid)s for energy and the environment. *Poly. Int.* **2017**, *66* (8), 1119–1128.
- (14) Mecerreyes, D. Polymeric ionic liquids: Broadening the properties and applications of polyelectrolytes. *Prog. Polym. Sci.* **2011**, *36* (12), 1629–1648.
- (15) Qian, W.; Texter, J.; Yan, F. Frontiers in poly(ionic liquid)s: syntheses and applications. *Chem. Soc. Rev.* **2017**, *46* (4), 1124–1159.
- (16) Qiang, Y.; Zhang, S.; Guo, L.; Zheng, X.; Xiang, B.; Chen, S. Experimental and theoretical studies of four allyl imidazolium-based ionic liquids as green inhibitors for copper corrosion in sulfuric acid. *Corros. Sci.* **2017**, *119*, 68–78.
- (17) Niskanen, J.; Tousignant, M. N.; Peltekoff, A. J.; Lessard, B. H. 1,2,3-Triazole based poly(ionic liquids) as solid dielectric materials. *Polymer* **2021**, *212*, 123144.
- (18) Lee, M.; Choi, U. H.; Colby, R. H.; Gibson, H. W. Ion Conduction in Imidazolium Acrylate Ionic Liquids and their Polymers. *Chem. Mater.* **2010**, *22* (21), 5814–5822.
- (19) Haruna, K.; Obot, I. B.; Ankah, N. K.; Sorour, A. A.; Saleh, T. A. Gelatin: A green corrosion inhibitor for carbon steel in oil well acidizing environment. *J. Mol. Liq.* **2018**, *264*, 515–525.
- (20) Atta, A. M.; El-Mahdy, G. A.; Allohedan, H. A.; Abdullah, M. Poly(ionic liquid) based on modified ionic polyacrylamide for inhibition steel corrosion in acid solution. *Int. J. Electrochem. Sci.* **2015**, *10*, 10389–10401.
- (21) Taghavikish, M.; Dutta, N. K.; Roy Choudhury, N. Emerging Corrosion Inhibitors for Interfacial Coating. *Coatings* **2017**, *7* (12), 217.
- (22) Abdul Rahiman, A. F. S.; Sethumanickam, S. Corrosion inhibition, adsorption and thermodynamic properties of poly(vinyl alcohol-cysteine) in molar HCl. *Arabian J. Chem.* **2017**, *10*, S3358–S3366.
- (23) Umoren, S. A.; Solomon, M. M. Polymeric Corrosion Inhibitors for Oil and Gas Industry. In *Corrosion Inhibitors in the Oil and Gas Industry*, 1st ed.; Saji, V. S.; Umoren, S. A., Ed.; Wiley-VCH, 2020; pp 303–320.
- (24) Umoren, S. A.; Obot, I. B. Polyvinylpyrrolidone and Polyacrylamide as Corrosion Inhibitors for Mild Steel in Acidic Medium. *Surf. Rev. Lett.* **2008**, *15* (03), 277–286.
- (25) Khairou, K. S.; El-Sayed, A. Inhibition effect of some polymers on the corrosion of cadmium in a hydrochloric acid solution. *J. Appl. Polym. Sci.* **2003**, *88* (4), 866–871.
- (26) Kamali Ardakani, E.; Kowsari, E.; Ehsani, A. Imidazolium-derived polymeric ionic liquid as a green inhibitor for corrosion inhibition of mild steel in 1.0 M HCl: Experimental and computational study. *Colloids Surf., A* **2020**, *586*, 124195.
- (27) Likhanova, N. V.; López-Prados, N.; Guzmán-Lucero, D.; Olivares-Xometl, O.; Lijanová, I. V.; Arellanes-Lozada, P.; Arriola-Morales, J. Some polymeric imidazolates from alkylimidazolium as corrosion inhibitors of API SL X52 steel in production water. *J. Adhes. Sci. Technol.* **2022**, *36* (8), 845–874.
- (28) de Sampaio, M. T. G.; Fernandes, C. M.; de Souza, G. G. P.; Carvalho, E. S.; Velasco, J. A. C.; Silva, J. C. M.; Alves, O. C.; Ponzio, E. A. Evaluation of Aqueous Extract of *Mandevilla fragrans* Leaves as Environment-Friendly Corrosion Inhibitor for Mild Steel in Acid Medium. *J. Bio Tribo Corros.* **2021**, *7* (1), 14.
- (29) Rahimi, A.; Abdouss, M.; Farhadian, A.; Guo, L.; Neshati, J. Development of a Novel Thermally Stable Inhibitor Based on Furfuryl Alcohol for Mild Steel Corrosion in a 15% HCl Medium for Acidizing Application. *Ind. Eng. Chem. Res.* **2021**, *60* (30), 11030–11044.
- (30) Zhang, J.; Zhang, L.; Tao, G.; Chen, N. Inhibition Effect and Adsorption Behavior of Two Imidazolium-based Ionic Liquids on X70 Steel in Sulfuric Acid Solution. *Int. J. Electrochem. Sci.* **2018**, *13*, 8645–8656.
- (31) Arellanes-Lozada, P.; Olivares-Xometl, O.; Likhanova, N. V.; Lijanová, I. V.; Vargas-García, J. R.; Hernández-Ramírez, R. E. Adsorption and performance of ammonium-based ionic liquids as corrosion inhibitors of steel. *J. Mol. Liq.* **2018**, *265*, 151–163.
- (32) Wang, X.; Yang, H.; Wang, F. An investigation of benzimidazole derivative as corrosion inhibitor for mild steel in different concentration HCl solutions. *Corros. Sci.* **2011**, *53* (1), 113–121.
- (33) Obot, I. B.; Madhankumar, A. Synergistic effect of iodide ion addition on the inhibition of mild steel corrosion in 1 M HCl by 3-amino-2-methylbenzylalcohol. *Mater. Chem. Phys.* **2016**, *177*, 266–275.
- (34) Corrales Luna, M.; Le Manh, T.; Cabrera Sierra, R.; Medina Flores, J. V.; Lartundo Rojas, L.; Arce Estrada, E. M. Study of corrosion behavior of API SL X52 steel in sulfuric acid in the presence of ionic liquid 1-ethyl 3-methylimidazolium thiocyanate as corrosion inhibitor. *J. Mol. Liq.* **2019**, *289*, 111106.
- (35) Gómez-Sánchez, G.; Likhanova, N. V.; Arellanes-Lozada, P.; Arriola-Morales, J.; Nava, N.; Olivares-Xometl, O.; Lijanová, I. V.; Corro, G. Electrochemical, surface and 1018-steel corrosion product characterization in sulfuric acid with new imidazole-derived inhibitors. *Int. J. Electrochem. Sci.* **2019**, *14*, 9255–9272.
- (36) Amin, M. A.; Khaled, K. F.; Fadl-Allah, S. A. Testing validity of the Tafel extrapolation method for monitoring corrosion of cold rolled steel in HCl solutions - Experimental and theoretical studies. *Corros. Sci.* **2010**, *52* (1), 140–151.
- (37) Furtado, L. B.; Nascimento, R. C.; Henrique, F. J. F. S.; Guimarães, M. J. O. C.; Rocha, J. C.; Ponciano, J. A. C.; Seidl, P. R. Effects of temperature, concentration and synergism on green Schiff bases synthesized from vanillin in applications as corrosion inhibitors for carbon steel in well stimulation. *J. Pet. Sci. Eng.* **2022**, *213*, 110401.
- (38) Saraswat, V.; Yadav, M. Improved corrosion resistant performance of mild steel under acid environment by novel carbon dots as green corrosion inhibitor. *Colloids Surf., A* **2021**, *627*, 127172.
- (39) Odusote, J. K.; Asafa, T. B.; Oseni, J. G.; Adeleke, A. A.; Adediran, A. A.; Yahya, R. A.; Abdul, J. M.; Adedayo, S. A. Inhibition efficiency of gold nanoparticles on corrosion of mild steel, stainless steel and

- aluminium in 1M HCl solution. *Mater. Today: Proc.* **2021**, *38*, 578–583.
- (40) Dkhireche, N.; Galai, M.; Ouakki, M.; Rbaa, M.; Ech-chihbi, E.; Lakhri, B.; EbnTouhami, M. Electrochemical and theoretical study of newly quinoline derivatives as a corrosion inhibitors adsorption on mild steel in phosphoric acid media. *Inorg. Chem. Commun.* **2020**, *121*, 108222.
- (41) León, L. L.; Rodríguez, M. V.; Cruz, V. R.; Calderón, F. A.; García, S. P. Corrosion of carbon steel in presence of hydrocarbon. *Int. J. Electrochem. Sci.* **2011**, *6*, 3497–3507.
- (42) El Asri, A.; Jmiai, A.; Mohamed Rguiti, M.; Oukhrib, R.; Abbeche, K.; Zejli, H.; Hilali, M.; Bourzi, H.; Bazzi, L.; El Issami, S. Computational and experimental studies of the inhibitory effect of imidazole derivatives for the corrosion of copper in an acid medium. *J. Mol. Liq.* **2022**, *345*, 117813.
- (43) Arellanes-Lozada, P.; Díaz-Jiménez, V.; Hernández-Cocolezzi, H.; Nava, N.; Olivares-Xometl, O.; Likhanova, N. V. Corrosion inhibition properties of iodide ionic liquids for API 5L X52 steel in acid medium. *Corros. Sci.* **2020**, *175*, 108888.
- (44) Porcayo-Calderon, J.; Casales-Diaz, M.; Rivera-Grau, L. M.; Ortega-Toledo, D. M.; Ascencio-Gutierrez, J. A.; Martinez-Gomez, L. Effect of the Diesel, Inhibitor, and CO₂ Additions on the Corrosion Performance of 1018 Carbon Steel in 3% NaCl Solution. *J. Chem.* **2014**, *2014*, 1–10.
- (45) Meeusen, M.; Zardet, L.; Homborg, A. M.; Lekka, M.; Andreatta, F.; Fedrizzi, L.; Boelen, B.; Mol, J. M. C.; Terry, H. The effect of time evolution and timing of the electrochemical data recording of corrosion inhibitor protection of hot-dip galvanized steel. *Corros. Sci.* **2020**, *173*, 108780.
- (46) El-Lateef, H. M. A.; El-Sayed, A.-R.; Mohran, H. S.; Shilkamy, H. A. S. Corrosion inhibition and adsorption behavior of phytic acid on Pb and Pb-In alloy surfaces in acidic chloride solution. *Int. J. Ind. Chem.* **2019**, *10* (1), 31–47.
- (47) Branzoi, I. V.; Iordoc, M.; Codescu, M. Electrochemical studies on the stability and corrosion resistance of new zirconium-based alloys for biomedical applications. *Surf. Interface Anal.* **2008**, *40* (3–4), 167–173.
- (48) Tan, Z.; Yang, L.; Zhang, D.; Wang, Z.; Cheng, F.; Zhang, M.; Jin, Y. Development mechanism of internal local corrosion of X80 pipeline steel. *J. Mater. Sci. Technol.* **2020**, *49*, 186–201.
- (49) Singh, A. K.; Shukla, S. K.; Quraishi, M. Corrosion behaviour of mild steel in sulphuric acid solution in presence of ceftazidime. *Int. J. Electrochem. Sci.* **2011**, *6*, 5802–5814.
- (50) Rugmini Ammal, P.; Prajila, M.; Joseph, A. Effect of substitution and temperature on the corrosion inhibition properties of benzimidazole bearing 1, 3, 4-oxadiazoles for mild steel in sulphuric acid: Physicochemical and theoretical studies. *J. Environ. Chem. Eng.* **2018**, *6* (1), 1072–1085.
- (51) Qiang, Y.; Zhang, S.; Wang, L. Understanding the adsorption and anticorrosive mechanism of DNA inhibitor for copper in sulfuric acid. *Appl. Surf. Sci.* **2019**, *492*, 228–238.
- (52) Mobin, M.; Basik, M.; Aslam, J. Pineapple stem extract (Bromelain) as an environmental friendly novel corrosion inhibitor for low carbon steel in 1 M HCl. *Measurement* **2019**, *134*, 595–605.
- (53) Li, H.; Zhang, S.; Qiang, Y. Corrosion retardation effect of a green cauliflower extract on copper in H₂SO₄ solution: Electrochemical and theoretical explorations. *J. Mol. Liq.* **2021**, *321*, 114450.
- (54) Kshama Shetty, S.; Nityananda Shetty, A. Eco-friendly benzimidazolium based ionic liquid as a corrosion inhibitor for aluminum alloy composite in acidic media. *J. Mol. Liq.* **2017**, *225*, 426–438.
- (55) Zhang, Q. H.; Hou, B. S.; Xu, N.; Xiong, W.; Liu, H. F.; Zhang, G. A. Effective inhibition on the corrosion of X65 carbon steel in the oilfield produced water by two Schiff bases. *J. Mol. Liq.* **2019**, *285*, 223–236.
- (56) Kissi, M.; Bouklah, M.; Hammouti, B.; Benkaddour, M. Establishment of equivalent circuits from electrochemical impedance spectroscopy study of corrosion inhibition of steel by pyrazine in sulphuric acid solution. *Appl. Surf. Sci.* **2006**, *252* (12), 4190–4197.
- (57) Patel, A. S.; Panchal, V. A.; Mudaliar, G. V.; Shah, N. K. Impedance spectroscopic study of corrosion inhibition of Al-Pure by organic Schiff base in hydrochloric acid. *J. Saudi Chem. Soc.* **2013**, *17* (1), 53–59.
- (58) Haldhar, R.; Prasad, D.; Saxena, A. Armoracia rusticana as sustainable and eco-friendly corrosion inhibitor for mild steel in 0.5M sulphuric acid: Experimental and theoretical investigations. *J. Environ. Chem. Eng.* **2018**, *6* (4), 5230–5238.
- (59) Zuriaga-Monroy, C.; Oviedo-Roa, R.; Montiel-Sánchez, L. E.; Vega-Paz, A.; Marín-Cruz, J.; Martínez-Magadán, J.-M. Theoretical Study of the Aliphatic-Chain Length's Electronic Effect on the Corrosion Inhibition Activity of Methylimidazole-Based Ionic Liquids. *Ind. Eng. Chem. Res.* **2016**, *55* (12), 3506–3516.
- (60) Farag, A. A.; Noor El-Din, M. R. The adsorption and corrosion inhibition of some nonionic surfactants on API X65 steel surface in hydrochloric acid. *Corros. Sci.* **2012**, *64*, 174–183.
- (61) Foo, K. Y.; Hameed, B. H. Insights into the modeling of adsorption isotherm systems. *Chem. Eng. J.* **2010**, *156* (1), 2–10.
- (62) Fernandes, C. M.; Alvarez, L. X.; dos Santos, N. E.; Maldonado Barrios, A. C.; Ponzio, E. A. Green synthesis of 1-benzyl-4-phenyl-1H-1,2,3-triazole, its application as corrosion inhibitor for mild steel in acidic medium and new approach of classical electrochemical analyses. *Corros. Sci.* **2019**, *149*, 185–194.
- (63) Papavinasam, S. Corrosion Inhibitors. In *Uhlig's Corrosion Handbook*; Revie, R.W., Ed.; John Wiley & Sons, 2011; pp 1021–1032.
- (64) Solomon, M. M.; Umoren, S. A.; Quraishi, M. A.; Jafar Mazumder, M. A. Corrosion inhibition of N80 steel in simulated acidizing environment by N-(2-(2-pentadecyl-4,5-dihydro-1H-imidazol-1-yl) ethyl) palmitamide. *J. Mol. Liq.* **2019**, *273*, 476–487.
- (65) Khadom, A. A.; Abd, A. N.; Ahmed, N. A. Xanthium strumarium leaves extracts as a friendly corrosion inhibitor of low carbon steel in hydrochloric acid: Kinetics and mathematical studies. *S. Afr. J. Chem. Eng.* **2018**, *25*, 13–21.
- (66) Yadav, D. K.; Maiti, B.; Quraishi, M. A. Electrochemical and quantum chemical studies of 3,4-dihydropyrimidin-2(1H)-ones as corrosion inhibitors for mild steel in hydrochloric acid solution. *Corros. Sci.* **2010**, *52* (11), 3586–3598.
- (67) Döner, A.; Solmaz, R.; Özcan, M.; Kardas, G. Experimental and theoretical studies of thiazoles as corrosion inhibitors for mild steel in sulphuric acid solution. *Corros. Sci.* **2011**, *53* (9), 2902–2913.
- (68) Ikpeseni, S. C.; Odu, G. O.; Owamah, H. I.; Onochie, P. U.; Ukala, D. C. Thermodynamic Parameters and Adsorption Mechanism of Corrosion Inhibition in Mild Steel Using Jatropha Leaf Extract in Hydrochloric Acid. *Arabian J. Sci. Eng.* **2021**, *46* (8), 7789–7799.
- (69) Chen, Z.; Fadhil, A. A.; Chen, T.; Khadom, A. A.; Fu, C.; Fadhil, N. A. Green synthesis of corrosion inhibitor with biomass platform molecule: Gravimetric, electrochemical, morphological, and theoretical investigations. *J. Mol. Liq.* **2021**, *332*, 115852.
- (70) Thoume, A.; Elmaksoudi, A.; Left, D. B.; Achagar, R.; Irahil, I. N.; Dakir, M.; Azzi, M.; Zertoubi, M. Dibenzylidenecyclohexanone as a New Corrosion Inhibitor of Carbon Steel in 1 M HCl. *J. Bio Tribol Corros.* **2021**, *7* (4), 130.
- (71) Khamaysa, O. M. A.; Selatnia, I.; Lgaz, H.; Sid, A.; Lee, H.-S.; Zeghache, H.; Benahmed, M.; Ali, I. H.; Mosset, P. Hydrazone-based green corrosion inhibitors for API grade carbon steel in HCl: Insights from electrochemical, XPS, and computational studies. *Colloids Surf., A* **2021**, *626*, 127047.
- (72) Benali, O.; Zebida, M.; Benhiba, F.; Zarrouk, A.; Maschke, U. Carbon steel corrosion inhibition in H₂SO₄ 0.5 M medium by thiazole-based molecules: Weight loss, electrochemical, XPS and molecular modeling approaches. *Colloids Surf., A* **2021**, *630*, 127556.
- (73) Cao, S.; Liu, D.; Zhang, P.; Yang, L.; Yang, P.; Lu, H.; Gui, J. Green Brønsted acid ionic liquids as novel corrosion inhibitors for carbon steel in acidic medium. *Sci. Rep.* **2017**, *7* (1), 8773.
- (74) El-Katori, E. E.; Nessim, M. I.; Deyab, M. A.; Shalabi, K. Electrochemical, XPS and theoretical examination on the corrosion inhibition efficacy of stainless steel via novel imidazolium ionic liquids in acidic solution. *J. Mol. Liq.* **2021**, *337*, 116467.

- (75) Yang, D.; Liu, S. H.; Shao, Y. P.; Xu, S. D.; Zhao, L. L.; Liao, Q. Q.; Ge, H. H. Electrochemical and XPS studies of alkyl imidazoline on the corrosion inhibition of carbon steel in citric acid solution. *Corros. Rev.* **2016**, *34* (5–6), 295–304.
- (76) Taufiq, A.; Saputro, R. E.; Susanto, H.; Hidayat, N.; Sunaryono, S.; Amrillah, T.; Wijaya, H. W.; Mufti, N.; Simanjuntak, F. M. Synthesis of Fe₃O₄/Ag Nanohybrid Ferrofluids and Their Applications as Antimicrobial and Antifibrotic Agents. *Heliyon* **2020**, *6* (12), e05813.
- (77) Pour-Ali, S.; Hejazi, S. Tiazofurin drug as a new and non-toxic corrosion inhibitor for mild steel in HCl solution: Experimental and quantum chemical investigations. *J. Mol. Liq.* **2022**, *354*, 118886.
- (78) Wang, H.; Gao, M.; Guo, Y.; Yang, Y.; Hu, R. A natural extract of tobacco rob as scale and corrosion inhibitor in artificial seawater. *Desalination* **2016**, *398*, 198–207.
- (79) Wang, X.; Huang, A.; Lin, D.; Talha, M.; Liu, H.; Lin, Y. Imidazolium-based Ionic Liquid as Efficient Corrosion Inhibitor for AA 6061 Alloy in HCl Solution. *Materials* **2020**, DOI: 10.3390/ma13204672.
- (80) Saraswat, V.; Kumari, R.; Yadav, M. Novel carbon dots as efficient green corrosion inhibitor for mild steel in HCl solution: Electrochemical, gravimetric and XPS studies. *J. Phys. Chem. Solids* **2022**, *160*, 110341.
- (81) Cui, M.; Yu, Y.; Zheng, Y. Effective Corrosion Inhibition of Carbon Steel in Hydrochloric Acid by Dopamine-Produced Carbon Dots. *Polymers* **2021**, *13* (12), 1923.
- (82) Singh, P.; Srivastava, V.; Quraishi, M. A. Novel quinoline derivatives as green corrosion inhibitors for mild steel in acidic medium: Electrochemical, SEM, AFM, and XPS studies. *J. Mol. Liq.* **2016**, *216*, 164–173.
- (83) Fu, S. Experimental and Theoretical Investigation of Corrosion Inhibition Effect of Multi-Active Compounds on Mild Steel in 1 M HCl. *Int. J. Electrochem. Sci.* **2019**, *6855*–6873.
- (84) El-Haddad, M. A. M.; Bahgat Radwan, A.; Sliem, M. H.; Hassan, W. M. I.; Abdullah, A. M. Highly efficient eco-friendly corrosion inhibitor for mild steel in 5 M HCl at elevated temperatures: experimental & molecular dynamics study. *Sci. Rep.* **2019**, *9* (1), 3695.
- (85) López, D. A.; Schreiner, W. H.; de Sánchez, S. R.; Simison, S. N. The influence of carbon steel microstructure on corrosion layers: An XPS and SEM characterization. *Appl. Surf. Sci.* **2003**, *207* (1), 69–85.
- (86) el Azzouzi, M.; Azzaoui, K.; Warad, I.; Hammouti, B.; Shityakov, S.; Sabbahi, R.; Saoiabi, S.; Moulay Hfid, Y.; Akartasse, N.; Jodeh, S.; et al. Moroccan, Mauritania, and Senegalese gum Arabic variants as green corrosion inhibitors for mild steel in HCl: Weight loss, Electrochemical, AFM and XPS studies. *J. Mol. Liq.* **2022**, *347*, 118354.
- (87) Luo, W.; Zhang, S.; Wang, X.; Gao, F.; Li, H. Ionic macromolecules based on non-halide counter anions for super prevention of copper corrosion. *J. Mol. Liq.* **2022**, *349*, 118156.
- (88) Bentiss, F.; Outirite, M.; Traisnel, M.; Vezin, H.; Lagrenée, M.; Hammouti, B.; Al-Deyab, S.; Jama, C. Improvement of corrosion resistance of carbon steel in hydrochloric acid medium by 3, 6-bis (3-pyridyl) pyridazine. *Int. J. Electrochem. Sci.* **2012**, *7* (2), 1699–1723.
- (89) Solmaz, R.; Mert, M. E.; Kada, S. G.; Yazici, B.; Erbil, M. Adsorption and Corrosion Inhibition Effect of 1,1-Thiocarbonyldiimidazole on Mild Steel in H₂SO₄ Solution and Synergistic Effect of Iodide Ion. *Acta Phys.-Chim. Sin.* **2008**, *24* (07), 1185–1191.
- (90) Likhanova, N. V.; Domínguez-Aguilar, M. A.; Olivares-Xometl, O.; Nava-Entzana, N.; Arce, E.; Dorantes, H. The effect of ionic liquids with imidazolium and pyridinium cations on the corrosion inhibition of mild steel in acidic environment. *Corros. Sci.* **2010**, *52* (6), 2088–2097.
- (91) Jeyaprabha, C.; Sathiyarayanan, S.; Venkatachari, G. Influence of halide ions on the adsorption of diphenylamine on iron in 0.5M H₂SO₄ solutions. *Electrochim. Acta* **2006**, *51* (19), 4080–4088.
- (92) Margarella, A. M.; Perrine, K. A.; Lewis, T.; Faubel, M.; Winter, B.; Hemminger, J. C. Dissociation of Sulfuric Acid in Aqueous Solution: Determination of the Photoelectron Spectral Fingerprints of H₂SO₄, HSO₄⁻, and SO₄²⁻ in Water. *J. Phys. Chem. C* **2013**, *117* (16), 8131–8137.
- (93) Verma, C.; Ebenso, E. E.; Quraishi, M. A. Ionic liquids as green corrosion inhibitors for industrial metals and alloys. In *Green Chemistry*, 1st ed.; Saleh, H. E.-D. M., Koller, M., Eds.; IntechOpen: London, 2018; pp 103–132.
- (94) Goyal, M.; Vashisht, H.; Hamed Alrefae, S.; Jain, R.; Kumar, S.; Kaya, S.; Guo, L.; Verma, C. Decyltriphenylphosphonium bromide containing hydrophobic alkyl-chain as a potential corrosion inhibitor for mild steel in sulfuric acid: Theoretical and experimental studies. *J. Mol. Liq.* **2021**, *336*, 116166.
- (95) Ohtsuka, T. Corrosion Protection of Steels by Conducting Polymer Coating. *Int. J. Corros.* **2012**, *2012*, 915090.
- (96) Wu, Q.; Jia, X.; Wong, M. Effects of number, type and length of the alkyl-chain on the structure and property of indazole derivatives used as corrosion inhibitors. *Mater. Today Chem.* **2022**, *23*, 100636.
- (97) Mandal, S.; Murmu, M.; Sengupta, S.; Baranwal, R.; Hazra, A.; Hirani, H.; Banerjee, P. Effect of molecular chain length on the tribological properties of two diazomethine functionalised molecules as efficient surface protective lubricant additive: experimental and in silico investigation. *J. Adhes. Sci. Technol.* **2022**, 1–27.
- (98) Liang, Y.; Gao, F.; Wang, L.; Lin, S. In-situ monitoring of polyelectrolytes adsorption kinetics by electrochemical impedance spectroscopy: Application in fabricating nanofiltration membranes via layer-by-layer deposition. *J. Membr. Sci.* **2021**, *619*, 118747.
- (99) Guzmán-Lucero, D.; Castillo-Acosta, S.; Martínez-Palou, R. Glycerol Carbonate Synthesis Using Poly(1-alkyl-3-vinylimidazolium) Imidazolates as Catalysts. *ChemistrySelect* **2020**, *5* (43), 13694–13702.
- (100) Guzmán-Lucero, D.; Olivares-Xometl, O.; Martínez-Palou, R.; Likhanova, N. V.; Domínguez-Aguilar, M. A.; Garibay-Febles, V. Synthesis of Selected Vinylimidazolium Ionic Liquids and Their Effectiveness as Corrosion Inhibitors for Carbon Steel in Aqueous Sulfuric Acid. *Ind. Eng. Chem. Res.* **2011**, *50* (12), 7129–7140.
- (101) Minsk, L. M.; Kotlarchik, C.; Meyer, G. N.; Kenyon, W. O. Imidization during polymerization of acrylamide **1974**, *12* (1), 133–140.
- (102) Calvillo-Muñoz, E. Y.; Vega-Paz, A.; Guzman-Lucero, D.; Lijanova, I. V.; Olivares-Xometl, O.; Likhanova, N. V. Synthesis of water-soluble ionic terpolymers by inverse microemulsion and solution polymerization methods. *RSC Adv.* **2022**, *12* (20), 12273–12282.
- (103) Biswas, Y.; Banerjee, P.; Mandal, T. K. From Polymerizable Ionic Liquids to Poly(ionic liquid)s: Structure-Dependent Thermal, Crystalline, Conductivity, and Solution Thermoresponsive Behaviors. *Macromolecules* **2019**, *52* (3), 945–958.
- (104) Jafar Mazumder, M. A. New Amino Acid Based Zwitterionic Polymers as Promising Corrosion Inhibitors of Mild Steel in 1 M HCl. *Coatings* **2019**, *9*, 675.
- (105) Olivares-Xometl, O.; Álvarez-Álvarez, E.; Likhanova, N. V.; Lijanova, I. V.; Hernández-Ramírez, R. E.; Arellanes-Lozada, P.; Varela-Caselis, J. L. Synthesis and corrosion inhibition mechanism of ammonium-based ionic liquids on API 5L X60 steel in sulfuric acid solution. *J. Adhes. Sci. Technol.* **2018**, *32* (10), 1092–1113.
- (106) ASTM G1–03. *Standard Practice for Preparing, Cleaning, and Evaluating Corrosion Test Specimens*; West Conshohocken, PA, 2017. DOI: 10.1520/G0001-03R17E01.
- (107) ASTM G106–89. *Standard Practice for Verification of Algorithm and Equipment for Electrochemical Impedance Measurements*; West Conshohocken, PA, 2015. DOI: 10.1520/G0106-89R15.
- (108) ASTM G59–97. *Standard Test Method for Conducting Potentiodynamic Polarization Resistance Measurements*; West Conshohocken, PA, 2014. DOI: 10.1520/G0059-97R14.
- (109) ASTM G16–13. *Standard Guide for Applying Statistics to Analysis of Corrosion Data*; West Conshohocken, PA, 2019. DOI: 10.1520/G0016-13R19.2.
- (110) ASTM G31–72. *Standard Practice for Laboratory Immersion Corrosion Testing of Metals*; West Conshohocken, PA, 2004. DOI: 10.1520/G0031-72R04.